

**SYNCHRONIZATION REQUIREMENTS FOR DOWNLINK
COORDINATED MULTIPOINT JOINT TRANSMISSION**

A Thesis

Presented to the

Faculty of

San Diego State University

In Partial Fulfillment

of the Requirements for the Degree

Master of Science

in

Electrical Engineering

by

Amir Shahrokh Hejazi

Summer 2014

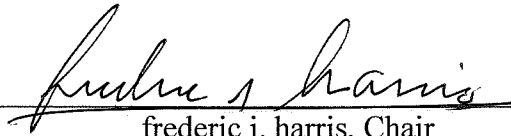
SAN DIEGO STATE UNIVERSITY

The Undersigned Faculty Committee Approves the

Thesis of Amir Shahrokh Hejazi:

Synchronization Requirements for Downlink Coordinated Multipoint Joint

Transmission



frederic j. harris, Chair

Department of Electrical and Computer Engineering



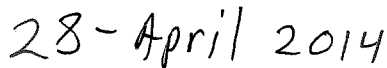
Mahasweta Sarkar

Department of Electrical and Computer Engineering



Christopher Paolini

Department of Computer Science



Approval Date

Copyright © 2014
by
Amir Shahrokh Hejazi
All Rights Reserved

DEDICATION

To family and friends
whom helped me to get
through my master.

ABSTRACT OF THE THESIS

Synchronization Requirements for Downlink Coordinated
Multipoint Joint Transmission

by

Amir Shahrokh Hejazi
Master of Science in Electrical Engineering
San Diego State University, 2014

This Master's Thesis aims to investigate the synchronization requirements for downlink Coordinated Multi-Point (CoMP) Joint Transmission in Long Term Evolution-Advanced (LTE-A) communication systems by utilizing mathematical proofs and MATLAB simulations. The purpose of the study is to enhance the signal to noise ratio of the cell edge users by using downlink Coordinated Multi-Point Joint Transmission scheme. This enables multiple base stations to transmit the same signal to the user equipment at the cell edge. The study will attempt to examine the system by using training symbols to estimate the channel for an accurate and efficient synchronization scheme. It will also attempt to derive a precise effect of time and frequency offset on the received signals. The Schmidl and Cox algorithm will be used for frame detection process at the receiver site, while the Zadoff-Chu sequence will be used as a reference signal for synchronization process.

TABLE OF CONTENTS

	PAGE
ABSTRACT	v
LIST OF TABLES	viii
LIST OF FIGURES	ix
ACKNOWLEDGMENTS	xi
CHAPTER	
1 INTRODUCTION	1
1.1 Background	1
1.2 Motivation	2
1.3 Organization	2
2 INTRODUCTION	3
2.1 Orthogonal Division Frequency Multiplexing Overview	3
2.2 Single Carrier–Frequency Division Multiple Access	6
2.3 LTE Frame Structure	7
2.4 Synchronization for OFDM Systems	7
2.4.1 Downlink Synchronization Process for LTE Systems	8
2.4.2 Coherent and Non-Coherent Detection	11
2.5 Coordinated Multi-Point Transmission and Reception	12
2.5.1 Uplink Transmission for CoMP Systems	13
2.5.2 Downlink Transmission for Comp Scheme	13
2.5.2.1 Clustering	14
2.5.2.2 Synchronization	14
2.5.2.3 channel estimation	16
2.5.2.4 Backhaul Link Network	17
3 SIMULATION AND RESULTS	19
3.1 Data Modulation	19
3.2 OFMD Packet	24
3.3 Channel Model	25

3.4 Synchronization Process	28
3.4.1 Automatic Gain Control.....	29
3.4.2 Schmidl and Cox Frame Detection Algorithm	31
3.4.3 Integer Time Offset Estimation	35
3.4.4 Fractional Time Offset Correction.....	36
3.4.5 Channel Estimation.....	38
4 CONCLUSION AND FUTURE WORK	42
REFERENCES	44
APPENDIX	
MATLAB SCRIPTS.....	46

LIST OF TABLES

	PAGE
Table 3.1. Channel Parameters	26
Table 3.2. Simulation Specifications	41

LIST OF FIGURES

	PAGE
Figure 2.1. Single subcarrier and multipoint subcarriers.....	4
Figure 2.2. Block diagram of transmitter and receiver for OFDM system.....	5
Figure 2.3. Type 1 LTE frame structure.	7
Figure 2.4. CoMP joint transmission appear as a multipath channels.....	12
Figure 2.5. CoMP joint transmissions scheme.....	14
Figure 2.6. CoMP JT is equivalent to MISO system.	15
Figure 2.7. OFDM Symbols with time offset.	16
Figure 3.1. Real parts (red line), imaginary parts (black line), and constellation diagram of QPSK symbol.	20
Figure 3.2. Frequency responses, shifting the spectrum, power spectrum, and time response of QPSK symbol.	21
Figure 3.3. Real parts (red line), imaginary parts (black line), and constellation diagram of 16 QAM symbol.	21
Figure 3.4. Frequency response, shifting the spectrum, power spectrum, and time response of 16 QAM symbol.	22
Figure 3.5. Constant Amplitude and Real and Imaginary Parts, Auto-Correlation, Phase of ZC Sequence.	23
Figure 3.6. Frequency response, shifting the spectrum, and time response of ZC sequence.	23
Figure 3.7. Normal CP versus Richard Van Nee's CP.	24
Figure 3.8. OFDM packet.	25
Figure 3.9. Transmitted signals with 28 and 45 samples of delayed from transmitted one and two, accordingly.	25
Figure 3.10. Magnitude and phase response of the ZC sequences after propagating through the multipath fading channel for transmitter one and two, respectively.	27
Figure 3.11. Frequency, time, and phase response of the two added signals.	27
Figure 3.12. The frequency, time, and phase response of the received signal after propagating through an AWGN channel.	28
Figure 3.13. Automatic gain control loop.....	29

Figure 3.14. Signal level at the output of AGC loop and the error estimation for LMS algorithm.	30
Figure 3.15. Block diagram for frame detection process, time offset estimation, and frequency offset estimation.	31
Figure 3.16. Auto-correlation and cross-correlation process for single transmitter and receiver.	33
Figure 3.17. Time metric estimator for single transmitter and receiver.	33
Figure 3.18. Auto-correlation and cross-correlation process for CoMP JT scheme.	34
Figure 3.19. Timing metric estimator for CoMP JT scheme.	34
Figure 3.20. Time offset estimation for downlink CoMP JT signals.	35
Figure 3.21. Block diagram of arbitrary resampling interpolator with two neighbor interpolation technique.	37
Figure 3.22. Signals at input and output of ARI for two neighbor interpolation technique.	37
Figure 3.23. Estimated channels via ZC sequence, phase response and frequency response of ZC sequence after equalization process.	39
Figure 3.24. Frequency response and constellation diagram of the QPSK Symbols for before and after Channel Equalization process.	39
Figure 3.25. Frequency response and constellation diagram of 16-QAM symbol for before and after channel equalization process.	40

ACKNOWLEDGMENTS

I would like to acknowledge and thank Dr. Fred Harris for his support and mentorship as his dedication to academia, research, and students is unmatched. It has been a privilege and an honor to work with such an inspiring professor.

CHAPTER 1

INTRODUCTION

The purpose of this study is to investigate the synchronization requirements for downlink Coordinated Multi-Point (CoMP) Joint Transmission (JT) systems. The study will evaluate the effects of the channel distortion, time offsets and Additive White Gaussian Noise (AWGN) on Orthogonal-Frequency-Division-Multiplexing (OFDM) signals for Long Term Evolution -Advanced (LTE-A) systems.

1.1 BACKGROUND

Mobile communication has an important role in the general public. Today's society heavily relies on smart phones for exchanging information and communication which includes: voice calls, text messaging, web browsing, multimedia, GPS, and video streaming to name a few. Therefore, it is essential to have a reliable wireless communication system. Long Term Evolution (LTE) is a standard wireless communication system used for high speed mobile communication worldwide. As the numbers of the mobile subscribers increases around the world, so does the demand on the advanced wireless communication systems. This demand has propelled the research in next generation mobile communication systems.

LTE-A is the newest generation of wireless mobile communication which is a major improvement of Long Term Evolution (LTE) systems. LTE-A has many advantages compared to the previous wireless mobile communication systems. Furthermore, LTE-A has been submitted to International Telecommunication Union (ITU) as a nominee for the Fourth Generation (4G) of mobile communication standards [1]. Coordinated Multi-Point (CoMP) transmission and reception is a promising technique for LTE-Advanced systems. Several studies have shown that Orthogonal Frequency Division Multiplexing (OFDM) carries an essential role in modern wireless communication systems due to its robustness against frequency/time-selective fading channel and high spectrum efficiency. In recent years, the combination of OFDM and CoMP transmission and reception has been recognized as a potential technique to support future broadband wireless communications systems [2].

1.2 MOTIVATION

The current literature on CoMP transmission/reception has not reached a consistent conclusion about the applicability of full implementation of the scheme for LTE-A. In practical scenarios, cell edge users generally have a lower Signal-to-Interference-Plus-Noise Ratio (SINR) causing degradation of the overall quality of service. This degradation can be due to the distance between the transmitter and receiver, noise interference, or multipath fading channels. One way to overcome these degradations and enhance the SINR of the received signal is to utilize downlink CoMP JT scheme.

1.3 ORGANIZATION

Chapter 2 of this thesis will provide a brief description of OFDM technology as well as outline the synchronization signals used for downlink transmission in LTE systems. It will also review synchronization requirements for downlink CoMP JT. Accordingly Chapter 3 will cover the simulation and results for synchronization in downlink CoMP JT schemes. In Chapter 4, conclusions and future directions for research will be discussed.

CHAPTER 2

INTRODUCTION

There are key elements which make LTE-A a more desirable candidate for wireless communication systems. Previous generations such as Third Generation Partnership Project (3GPP) Code Division Multiple Access (CDMA) and LTE have a slower data rate transfer for downlink and uplink signals. Furthermore, 3GPP LTE-A is a promising scheme to accomplish the goals for the 4th generation wireless communication systems. Currently some of the key features for LTE-A includes: peak data rates, spectrum efficiency, peak spectrum efficiency, spectrum use, latency, cell edge user throughput, average user throughput, and mobility. However, a great deal of work remains for implementation of these components in practical scenarios [3]. This chapter will cover some of these key factors more in depth.

2.1 ORTHOGONAL DIVISION FREQUENCY MULTIPLEXING OVERVIEW

Orthogonal Frequency Division Multiplexing (OFDM) is basis for LTE technology. Orthogonal Frequency Division Multiple Access (OFDMA) is an improvement of the OFDM system which allows data to be transmitted wirelessly by sharing the channel's bandwidth with multiple users simultaneously. This technology has been utilized for 3GPP LTE, WiMAX, and the Digital Video Broadcasting (DVB) systems. In LTE wireless communication systems OFDMA is used to transmit the downlink signals, while Single Carrier-Frequency Division Multiple Access (SC-FDMA) is used to transmit the uplink signals. SC-FDMA employs a single carrier modulation scheme to transmit the data that have lower Peak-to-Average-Power Ratio (PAPR) in comparison to the OFDMA modulation scheme. Even though SC-FDMA signals have lower power consumption compared to OFDMA transmissions, OFDMA signals are more robust against severe multipath fading channel.

OFDM technology carries many advantages for wireless communication systems. For instance, it transforms a frequency-selective wideband signal into a group of narrowband signals making them more robust against the time dispersive channel. At the same time,

OFDM signals preserve the orthogonality of the signals in the frequency domain [4]. Figure 2.1 depicts the spectrum of single carrier and multiple carriers of the OFDM signal. The frequency spacing of each subcarrier is $\Delta f = 1/T_u$ where T_u represents the time duration of each subcarrier. In OFDM technology, null of each subcarrier is the maximum of the neighboring subcarrier and subcarriers are orthogonal to each other.



Figure 2.1. Single subcarrier and multipoint subcarriers.

The two functions $a(x)$ and $b(x)$ are said to be orthogonal over the period of $[-T, T]$ if and only if they satisfy equation 2.1 shown below.

$$\int_{-T}^T a(x)b(x) = 0 \quad (2.1)$$

Modulation of information in wireless communication is defined as mapping of the data on phase, frequency, amplitude of carrying signals and/or any combination of those three [4]. Equation 2.2 represents a modulated OFDM signal $x(t)$,

$$x(t) = \sum_{m=0}^{N-1} a_m e^{-j2\pi\Delta f_s t} \quad (2.2)$$

Where a_m , Δf , N and t are complex number, subcarrier spacing, number of subcarriers, and the time interval of the transmitted signal respectively. Some of the basic characteristics of OFDM transmission are listed below [4]:

- In an OFDM system, there are a larger number of narrowband subcarriers utilized for transmission.
- Each subcarrier is equivalent to the Sinc-square-shaped in the frequency domain which is also equivalent to rectangular pulse-shape in the time domain.
- Subcarriers in the frequency domain are closely packed making the system more spectrum-efficient compared to earlier communication systems.

In OFDM systems, the Inverse Fast Fourier Transform (IFFT) is utilized at the transmitter site for the modulation process, while Fast Fourier Transform (FFT) is used at the receiver site for the demodulation process. The reasons IFFT and FFT process has been adopted for modulation and demodulation in OFDM systems is due to the low-complexity

implementation and computational efficiency. Figure 2.2 depicts the block diagram of the transmitter and receiver for OFDM systems.

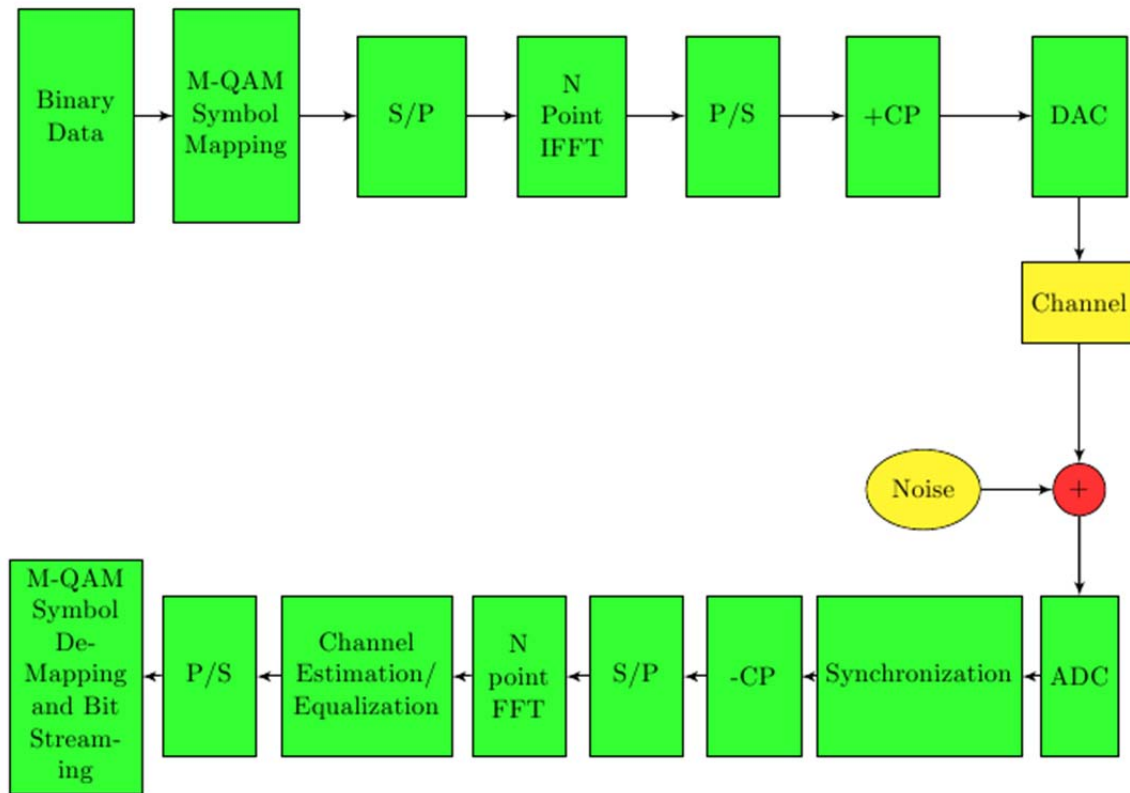


Figure 2.2. Block diagram of transmitter and receiver for OFDM system.

At the transmitter site, mapping of the data can occur via Quadrature Phase Shift Keying (QPSK) or 16-state Quadrature Amplitude Modulation (16 QAM) prior to the IFFT process. After mapping of the data, a large number of narrowband closely packed subcarriers are transformed into time domain signals by the IFFT process. In the time domain, the amplitude and phase of the sinusoid signals is used to represent the frequency domain symbols. Next, each block of N (number of IFFT points or coefficients) is generally preceded by a guard interval or Cyclic Prefix (CP). This process, by design, protects the signal against the delay spreading of the channel. Moreover, if the length of CP is not chosen accurately, the received signal will suffer from Inter-Symbol Interferences (ISI) and/or Inter-Carrier Interferences (ICI). The next phase of the transmission process is to convert the digital data to analog signals. This process is accomplished by a procedure known as Digital to Analog Converter (D/A). The received signals propagate through time dispersive (frequency

selective Fading) channel with the presence of Additive White Gaussian Noise (AWGN). Equation 2.3 represents a simplified version of the received signal at the time instance m ,

$$y_m = \sum_{l=0}^{L-1} x_m(n-l)h_m(l) + w_m(n) \quad (2.3)$$

Where x_m , h_m , and w_m represents the transmitted signal, channel impulse response, and Additive White Gaussian Noise respectively. At the receiver site, the Analog to Digital Converter (A/D) takes the continuous time and amplitude received signals and converts them to discrete time and amplitude digital signals. Next, a synchronization technique is used for the received signal in order to appropriately find the start of the frame and to estimate as well as correct any frequency and time offsets. This enables progression the FFT process. After converting the signals from the time domain to the frequency domain, channel estimation and channel equalization occurs. The last step of synchronization process consists of de-mapping of the data.

2.2 SINGLE CARRIER–FREQUENCY DIVISION MULTIPLE ACCESS

The fundamental conceptual difference between Single Carrier-Frequency Division Multiple Access (SC-FDMA) and OFDM transmission is that the SC-FDMA uses Discrete Fourier Transform Spread-OFDM (DFTS-OFDM) in addition to the normal OFDM modulation process. More specifically, the first step of the DFTS-OFDM modulation process is to perform a Discrete Fourier Transform (DFT) operation on the M -blocks of the data symbols. The output of DFT is then applied to the input of the OFDM modulator. In practical applications, the OFDM modulation process will be implemented in blocks of the N -points IFFT operation where $N > M$. Thus, the unused bins for DFT operation are set to zeroes. One of the advantages of SC-FDMA is the small variation within the instantaneous power of the transmitted signal. This is a consequence of the high degree of flexibility in the nominal bandwidth for the transmitted signal. Also, the bandwidth of SF-FDMA depends on the block size M , assuming the sampling frequency for the transmitted data is $f_s = \Delta f * N$, where the bandwidth of transmitted signal will be $BW = \frac{M}{N} f_s$. By varying M , the number of subcarriers for the DFT operation, the bandwidth of transmitted signal can be varied accordingly [4]. Furthermore, the presence of CP in the front of the SC-FDMA signal allows for low-complexity equalization of the signal in the frequency domain. The main advantage

of DFTS-OFDM is the low Peak-to-Average-Power Ratio (PAPR) which increases the efficiency of the power amplifier for the transmitter [4]. For these reasons, SC-FDMA is used for uplink transmissions.

2.3 LTE FRAME STRUCTURE

In 3GPP LTE systems two types of radio frame structures are utilized to carry out the data from the base station to the User Equipment (UE) or vice versa. The two different types of frame structures are Frequency Division Duplex mode (FDD) and Time Division Duplex mode (TDD) which fall into the categories of the type 1 and type 2 respectively [3]. In the FDD mode, the uplink and downlink transmission takes place on different frequency bands, whereas, in the TDD mode the uplink and downlink transmission occurs on the same frequency band. However, the signals are separated in the time domain by using different time slots. Explicitly, in the time domain the length of the radio frames is 10ms, each of the frames are divided into 10 subframes (at a length 1ms). Each subframe is divided into two equally sized slots with a length of 0.5ms. Each of these time slots contains 6 or 7 OFDM symbols depending on the length of CP. Figure 2.3 below depicts the radio frame structure for the LTE system [3].

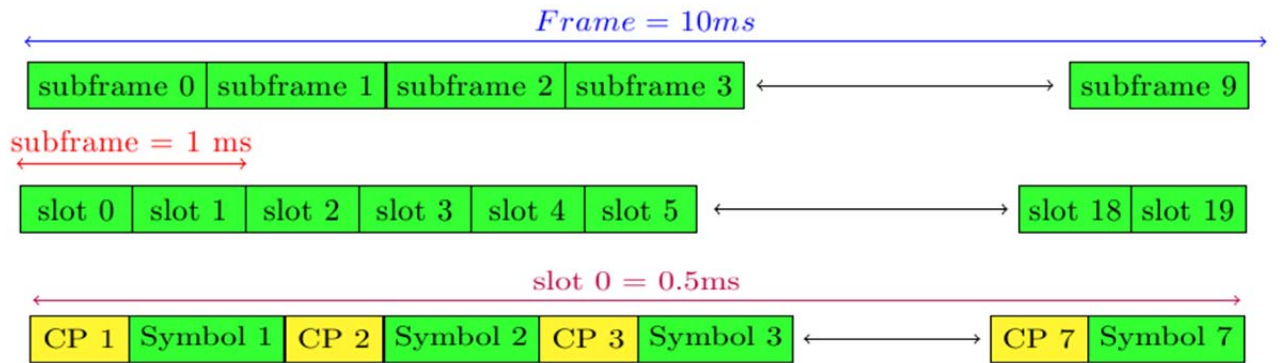


Figure 2.3. Type 1 LTE frame structure.

2.4 SYNCHRONIZATION FOR OFDM SYSTEMS

Synchronization is a vital part of OFDM systems because OFDM symbols are very sensitive to time and frequency offsets. The synchronization inaccuracies can occur because of a Symbol Timing Offset (STO) and/or a Carrier Frequency Offset (CFO). These errors stem from two main factors: the mismatch between the transmitter and receiver Local

Oscillators (LO) or impairment may arise from the Doppler frequency shift inside the channel [5]. Equation 2.4 illustrates the changes in the frequency or the Doppler shift of the transmitted signal, assuming the receiver is moving toward the transmitter.

$$f_D = v \frac{f_c}{c} \quad (2.4)$$

In the equation, f_D is the Doppler shift frequency, v is the speed of the UE, f_c is carrier frequency of the signal, and c is the speed of light [4]. It is important to minimize the impact of time and the frequency offset on the receive signals. This enables the receiver to identify the received symbols accurately, otherwise, it starts sampling a new frame at an incorrect time instant. The OFDM synchronization process can be categorized into data-aided and non-data-aided methods [5]. Furthermore, these two methods are normally implemented in two stages: the course synchronization for a rough estimation followed by a fine synchronization for a more precise estimation. In the case of data aided synchronization, pilot symbols or training sequences are utilized for time and frequency estimation. Although this technique has a high accuracy and low computation process, it reduces the overall bandwidth for data transmission. For the non-data-aided synchronization, the CP of OFDM symbols are used to estimate the time and frequency offset. This method does not waste any bandwidth or rate of transmission, but it suffers from an estimation range. This range is generally too small for the acquisition process [5]. For the remainder of this thesis, the data-aided method is used to describe the synchronization process.

2.4.1 Downlink Synchronization Process for LTE Systems

One of the most popular techniques for synchronization in OFDM systems is data aided method. In this method, the transmitter uses one or several pilot symbols that are known to both the transmitter and receiver for the synchronization process. The length of these training sequences (having predefined subcarriers and repeated patterns) depends on how fast the channel changes. Typically, at the receiver the correlation of these training sequences detects the start of the frame for OFDM symbols. The training sequences can also be exploited for time and frequency offset estimations. One of the most popular techniques for synchronization in OFDM systems is Schmidl and Cox Algorithm. It consists of two OFDM symbols $[A^+ A^+]$ with two identical halves which are placed at the beginning of the

frame [5]. Generally, it is desirable to design a training sequence with a good auto-correlation and cross-correlation properties. In practical applications, two commonly used sequences which satisfy the properties of aforementioned training sequences are the Zadoff-Chu (ZC) sequence and the Pseudo Noise (PN) sequence.

In LTE wireless communication systems, the downlink synchronization procedure is comprised of two synchronization sequences. The two synchronization sequences are known as the Primary Synchronization Signal (PSS) and the Secondary Synchronization Signal (SSS). Both sequences are transmitted on 62 of the 72 reserved subcarriers with the Direct Current (DC) subcarrier at the center bin. In the frequency domain, the synchronization signals require six Resource Blocks (RB) in order to complete the transmission process. Each RB consists of 12 subcarriers with an occupied bandwidth of 180 KHz. Thus, the required bandwidth for transmission of synchronization signals is $6 \times 180 \text{ KHz} = 1.08 \text{ MHz}$. In LTE systems, the ZC sequence is used for PSS due to its robustness against frequency offset, easy calculation process, and good correlation properties. The ZC sequences are complex signals in the form of an exponential function shown in Equation (2.5).

$$\begin{aligned} ZC_{N_{zc}}^u &= e^{(-j * u * \frac{n^2}{N_{zc}})} \text{ for } N_{zc} = \text{Even integer numbers} \\ ZC_{N_{zc}}^u &= e^{(-j * u * \frac{n * (n+1)}{N_{zc}})} \text{ for } N_{zc} = \text{Odd integer numbers} \end{aligned} \quad (2.5)$$

In Equation 2.5 N_{zc} denotes the length of the sequence and u is the root index of the ZC sequence. Normally, the root index u and the length of sequence N_{zc} are relative prime numbers which means that there is no common divider for both numbers except for 1. The ZC sequence has three main properties which are advantageous for the synchronization process in a LTE system. One of the properties of the ZC sequence is the Fourier Duality characteristics. This means, that the DFT of the ZC sequence is another ZC sequence. The second property of ZC sequence is the constant amplitude characteristic in both time and frequency domain. Due to this property, the PAPR of the transmitted sequences are limited since it only requires the phase of the sequence for the transmission process and not the amplitudes. The third advantage of the ZC sequence is the zero auto-correlation property which results in a unit impulse at zero lag and zeroes elsewhere. For these reasons the ZC sequence satisfies the Constant Amplitude Zero Autocorrelation (CAZAC) property. Later the receiver uses these properties to find the start of the frame and estimates any time and

frequency offsets of the received signals. Furthermore, the auto-correlation of any ZC sequence with a different root index will result in zero. Lastly, the cross-correlation function between any two ZC sequences has a constant magnitude response with a unit gain [6]. The physical layer in the LTE system has 504 unique cell identities which are divided into three possible physical cell identities (0, 1, or 2). Furthermore, each of these cell identities consists of 168 unique physical layer cell identity groups which can be denoted as,

$$N_{ID}^{cell} = 3N_{ID}^{(1)} + N_{ID}^{(2)} \quad (2.6)$$

Where $N_{ID}^{(1)}$ denotes the cell identity group (from 0 to 167) and $N_{ID}^{(2)}$ denotes the cell identities with 3 possible values (0, 1, and 2) [3]. For the primary synchronization process the ZC sequence is employed and for the secondary synchronization process the PN sequence is used. In the case of the PSS, the ZC sequence different root indices (u) are utilized to determine the cell identity which is denoted as follows [3],

$$ZC_{N_{zc}}^u = \begin{cases} u = 25 & \text{for } N_{ID}^{(2)} = 0 \\ u = 29 & \text{for } N_{ID}^{(2)} = 1 \\ u = 34 & \text{for } N_{ID}^{(2)} = 2 \end{cases} \quad (2.7)$$

For the Frequency Division Duplex frame type, PSS is always placed within the last OFDMA symbol of the first slot of subframes (0 and 5). In the case of Time Division Duplex frame type, PSS is placed within the third symbol of subframes (1 and 6) [4]. After the UE recognizes the cell identity via PSS (occurs within a 5ms time span of the radio frame timing) then the cells' identity group can be determined from the SSS. The SSS is generated in the frequency domain with the real values of +1 and -1. The SSS is a combination of two Pseudo Noise sequences which are scrambled with $N_{ID}^{(1)}$ and $N_{ID}^{(2)}$. The SSS is generated from two pseudorandom binary sequences each of a length of 31 samples. The two sequences $s_0^{(m_0)}$, $s_1^{(m_1)}$ are defined as two cyclic shifts of a primitive polynomial $x^5 + x^2 + 1$ over the finite field of the Galois field of two elements GF (2) where the indices m_0, m_1 denotes the cell-identity group as it is shown in following equation [3]:

$$\begin{aligned} s_0^{(m_0)} &= \hat{S}((n + m_0) \bmod 31) \\ s_1^{(m_1)} &= \hat{S}((n + m_1) \bmod 31) \end{aligned} \quad (2.8)$$

The next step consists of scrambling the two sequences with a binary scrambling code $(c_0(n), c_1(n))$ which is dependent on the physical layer of the cell identity $N_{ID}^{(2)}$. The sequence \hat{c} is generated from the primitive polynomial $x^5 + x^3 + 1$ over the finite field of GF (2). The two sequences $c_0(n), c_1(n)$ are given by the following equations [3]:

$$\begin{aligned} c_0 &= \hat{c} \left((n + N_{ID}^{(2)}) \bmod 31 \right) \\ c_1 &= \hat{c} \left((n + N_{ID}^{(2)}) \bmod 31 \right) \end{aligned} \quad (2.9)$$

Also, the SSS sequences in Equation 2.9 are scrambled with another pseudorandom binary sequence $(z_0^{m_0}, z_1^{m_1})$ with the primitive polynomial of $x^5 + x^4 + x^2 + 1$ over finite field GF (2) which are given by the following equations [3]:

$$\begin{aligned} z_0^{m_0} &= \hat{z} \left((n + (m_0 \bmod 8)) \bmod 31 \right) \\ z_1^{m_1} &= \hat{z} \left((n + (m_1 \bmod 8)) \bmod 31 \right) \end{aligned} \quad (2.10)$$

In the case of the FDD frame type, the SSS is placed within the second to the last symbol of the first slot of the subframe 0 and 5. In the case of the TDD frame type, the SSS is transmitted in the last symbols of subframe 0 and 5 [4]. The SSS uses different scrambling sequences when mapped to even or odd number of resource elements as it is shown in the following equations [3]:

$$\begin{aligned} d(2n) &= \begin{cases} s_0^{(m_0)} c_0(n) & \text{for even resource elements, in slot 0} \\ s_1^{(m_1)} c_0(n) & \text{for even resource elements, in slot 10} \end{cases} \\ d(2n + 1) &= \begin{cases} s_1^{(m_1)} c_1(n) z_1^{m_0}(n) & \text{for odd resource elements, in slot 0} \\ s_0^{(m_0)} c_1(n) z_1^{m_1}(N) & \text{for odd resource elements, in slot 10} \end{cases} \end{aligned} \quad (2.11)$$

Where $n = 0, 1, 2, 3 \dots 30$. In addition to synchronization sequences, reference signals or cell specific signals are used to have a more accurate knowledge of the channel for coherent demodulation. The reference signals are predefined values placed within the first and fifth OFDMA symbol of each slot and each reference symbol consists of three subcarriers [4].

2.4.2 Coherent and Non-Coherent Detection

Coherent and non-coherent detection has a significant role in the synchronization process for mobile wireless communication systems. Coherency in signal processing means that two random variables are correlated if there is a linear relationship between the two sets [7]. In other words, coherent signals have the same phase and frequency. For coherent

detection, the receiver takes advantage of the knowledge of the channel. More specifically, once the receiver compensates for any time or frequency offsets of the received signal then channel estimation and equalization of the signal will occur in the frequency domain. However, if the time and frequency error cannot be corrected by the receiver then non-coherent demodulation is implemented. In this case, the receiver uses the pilot signals only for the frame detection process [7].

2.5 COORDINATED MULTI-POINT TRANSMISSION AND RECEPTION

Coordinated Multi-Point (CoMP) transmission and reception is used in 4G LTE-A wireless communication systems to guarantee optimal performance for the cell edge users by transmitting and receiving data from multiple cell sites. Some of the advantages of LTE-A CoMP transmission/reception are to convert Inter-Cell Interference signals into useful signals for the cell edge users and to increase the received signal power. CoMP transmission and reception in mobile communication systems entails that the same data is transmitted simultaneously from multiple base stations to one terminal in order to increase the transmitted signal power. At the receiver site, the signal appears as if it propagates through multipath channels and is illustrated in Figure 2.4 [4].

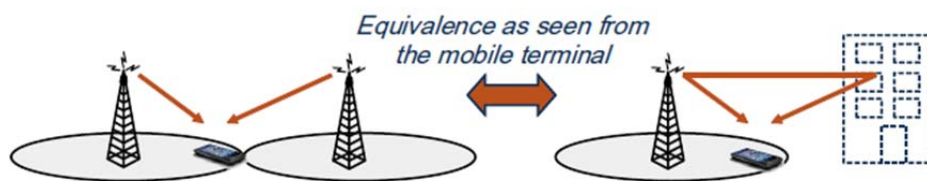


Figure 2.4. CoMP joint transmission appear as a multipath channels. Source: E. Dahlman et al., *4G LTE/LTE-Advanced for Mobile Broadband*. Burlington, MA: Academic Press, 2011.

Although, the downlink transmitted power is going to be increased with the use of the CoMP JT technique in LTE-A, the data rate can be considerably reduced if the cell edge user can utilize the received power for detecting and decoding the transmitted data. One way to mitigate this dilemma is to ensure that the transmissions from different base stations are identical and precisely time aligned. At the receiver site, the received signals appear as if

they were transmitted from a single base station but they propagate through severe multipath channels [4].

2.5.1 Uplink Transmission for CoMP Systems

There are two different categories of uplink CoMP schemes, category one which uses Joint Scheduling and category two uses Cooperative Interference Prediction. The basic idea behind joint scheduling is to make an environment where the cell sites cooperate with each other in order to mitigate the inter-cell interference signals. More specifically, base stations exchange channel information and scheduling decisions over the backhaul networks [2]. In category two the scheduling is performed individually by each base station, but the interference that occurred during the data transmission from the interfering terminals are estimated in a cooperative manner [2].

2.5.2 Downlink Transmission for CoMP Scheme

In the case of CoMP downlink transmission there are two classified categories: Coordinated Scheduling/Beamforming and Joint Processing (JP). In the case of Coordinated Scheduling/Beamforming, the data for the user is available at the serving base station while the user scheduling and Beamforming decisions are achieved through coordination among the assigned base stations for the CoMP scheme [8]. More specifically, coordinated scheduling among the assigned base stations for downlink CoMP schemes occurs by silencing the interfering base stations during the downlink transmission (from primary base station to the target UE).

In the Joint Processing CoMP scheme, multiple cell sites are accountable for Joint Transmissions of the same data to the targeted UE. By transmitting the same data through multiple cell sites, the Signal-to-Interference-Plus-Noise Ratio (SINR) of the received signal is increased. This technique can also be used to cancel the interfering signals coming from other Mobile Stations (MS). Figure 2.5 illustrates the basic idea for the downlink CoMP Joint Transmission.

The two cell sites that are assigned to the CoMP JT for the downlink signals form a CoMP cluster. Equation 2.12 exhibits the received signals seen by the receiver:

$$Y = X_1H_1 + X_2H_2 + W_1 + W_2 \quad (2.12)$$

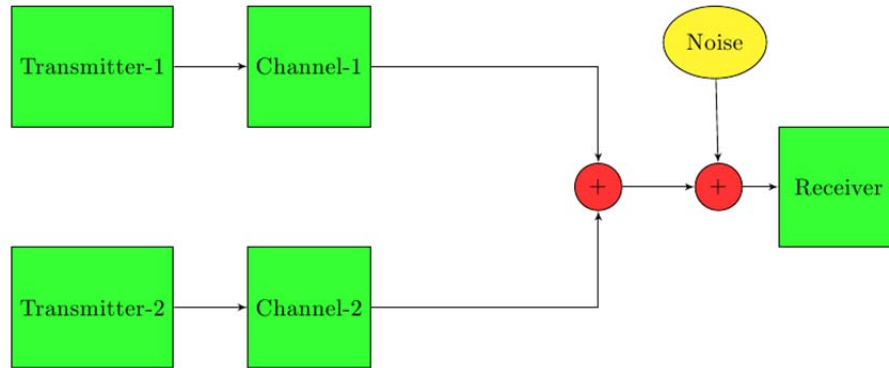


Figure 2.5. CoMP joint transmissions scheme.

Where X_{12} , H_{12} , W_{12} are the transmitted signals, channel frequency responses, and AWGNs for transmitter one and two respectively. Although, this technique enhances the over quality of the system, there are some practical challenges for implementation of the CoMP scheme. The obstacles in implementation of the CoMP technique are as follows: clustering, synchronization, channel estimation, and backhaul link network coordination.

2.5.2.1 CLUSTERING

In CoMP Joint Transmission of LTE-A suitable clusters the coordinated cell sites have to be determined in order to complete the transmission. This is accomplished through two methods by either static or dynamic methods. In static cooperative base stations (network defined scheme), several non-overlapping adjacent sectors are assigned to the cell-edge UE. Once these sectors are determined they will kept static for the rest of the transmission. In this case, the overall performance of the CoMP JT for cell edge Mobile Stations (MS) declines as the MS moves away from the clusters of the coordinated cell sites. On the contrary, by using a dynamic method the cell edge UE is free to select the cooperative cluster of cell sites for the CoMP JT scheme. In this method the cooperating cell clusters are setup adaptively according to the Radio Frequency (RF) channel and UE position. This setup enhances the overall performance of the system. While this method enhances the overall performance of the system, it also increased its complexity [8].

2.5.2.2 SYNCHRONIZATION

Synchronization amongst cooperative base stations plays an important role in the CoMP JT scheme. The cooperative base stations need to be synchronized in the time and

frequency domain in order to avoid Inter-Carrier and Inter-Symbol Interference. In practical applications, cooperation among base stations for Joint Transmission is the conceptual framework for Multiple-Input Single-Output (MISO) transmission. In MISO transmission, antennas located at the multiple cooperative base stations are considered as the inputs, while the antenna located at the UE is considered as the output. Figure 2.6 illustrates a distributed MISO system [9]. Imperfect synchronization amongst the cooperative cell-sites causes the Inter-Carrier Interference. In order to overcome the impact of the frequency offset in the received signals at the receiver site, Global Position Systems (GPS) synchronization is utilized to synchronize the transmitted signals among the cooperative base stations precisely. In other words, in the physical layer of the cooperative base stations local oscillators are controlled through the GPS via the backhaul link network [10].

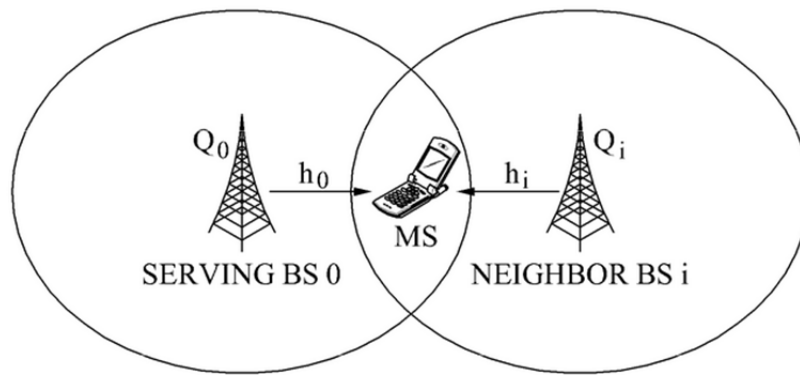


Figure 2.6. CoMP JT is equivalent to MISO system.

In practical settings, most phones are designed to have Code Division Multiple Access (CDMA) wireless technology for voice calling and text messaging between phones and LTE systems for web browsing and video streaming [11]. The assigned channel bandwidth for CDMA wireless technology is lower in comparison to LTE wireless technology. This is due to the fact that voice calling and text messaging does not require as much bandwidth for the transmission process. However, web browsing and video streaming uses larger amounts of bandwidth in order to complete the transmission process. In the case where two base stations are assigned for the CoMP JT scheme, the cell edge UE can use the CDMA and LTE system to synchronize to the base stations simultaneously. This method offers a more relaxing synchronization process among the cooperative cell sites. In this method, the UE is synchronized to the two base stations as opposed to the aforementioned

method where the UE is synchronized to the serving base station and the information for the JT is shared via the backhaul link network [11]. The downside to utilizing the CDMA and LTE system for synchronization with the cooperative base stations is the fact that the UE cannot use the CDMA system in certain situations during the synchronization process. For example, when the CDMA system is used for voice calling or text messaging the UE will not be able to synchronize to the base stations.

If the maximum distances between the assigned base stations for the downlink CoMP JT are beyond the length of the Cyclic Prefix then the receive signals will suffer from ISI [12]. For instance, if the assigned base stations for the Joint Transmission process transmit their signals simultaneously, then the signals will arrive at UE from BS_1 and BS_2 after delays of d_1/c and d_2/c respectively (c represents the speed of light). According to Hamza and Mark [12] in order to recover the received signal at the UE Equation 2.13 must be stratified otherwise the orthogonality of the subcarriers will be lost and will result in ISI.

$$0 \leq \frac{d_2 - d_1}{c} \leq T_{cp} - \tau_{max} \quad (2.13)$$

In this equation, T_{cp}, τ_{max} represents the period of Cyclic Prefix and the maximum delay spread of the channel. Figure 2.7 exhibits the event where the OFDM symbols from the two transmitters arrive with the maximum time offset causing ISI in the received signals.

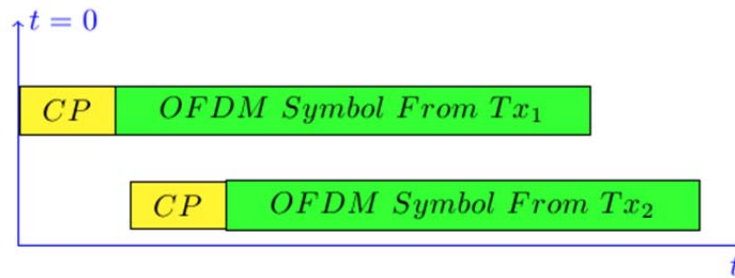


Figure 2.7. OFDM Symbols with time offset.

2.5.2.3 CHANNEL ESTIMATION

Channel estimation for downlink transmission occurs via the uplink training sequences by exploiting the channel reciprocity. If quasi-static frequency selective fading channels exist in the system, the channel remains constant during the downlink and uplink transmission. During uplink transmission the training symbols are transmitted to all of the cell sites and the estimated channel is shared among cooperative base stations via the X2

interface link [8]. When perfect synchronization is assumed among all the entities then the base stations obtain ideal channel knowledge at $t = 0$. Thus, simple zero Forcing Beamforming transmission would reverse the effect of the channel which is shown in Equation 2.14:

$$\begin{aligned} \mathbf{y} &= \mathbf{h}\mathbf{x}\mathbf{c} + \mathbf{w}, \\ \mathbf{c} &= \mathbf{h}^{-1} \end{aligned} \quad (2.14)$$

Where \mathbf{y} , \mathbf{x} , \mathbf{h} , \mathbf{c} , and \mathbf{w} are the received signal, transmitted signal, channel information, and AWGN respectively [10]. In the case where the synchronization among base stations is not ideal and/or there is large amount of frequency offset, there is no AWGN for the sake of simplicity. Equation 2.15 expresses the received signal:

$$r(n) = a(n) e^{j\phi_1(n)} + a(n)e^{j\phi_2(n)} \quad (2.15)$$

Where $r(n)$, $a(n)$, ϕ_1 , and ϕ_2 represents the received signal, modulated signal, and the frequency offsets for transmitters one and two respectively. In this scenario channel estimation is not possible because frequency offsets cannot be adequately corrected at the receiver site. As a result, the receiver proceeds with a non-coherent demodulation process.

2.5.2.4 BACKHAUL LINK NETWORK

In the CoMP JT approach, cell sites require a direct exchange of channel state information, control data, user data, and received signals via the X2 backhaul network in order to achieve fast and precise data transmission. Depending on the network backhaul structure the logic X2 interface could be a direct physical link or a multi-hop link [8]. In CoMP JT, the latency of X2 interface plays a major role in the transmission process. Because the connectivity among base stations occurs via the X2 interface and during the process of channel estimation and channel equalization, the knowledge of channel must not change. If the latency of the X2 interface exceeds the tolerated threshold then the channel information becomes outdated. In general there are two types of delays that affect the system: network node processing delay and line delay [8]. The latency for the X2 backhaul link should be below 1ms in order to avoid any performance derogation. As long as the propagation path among the cell sites are in the order of some kilometers then the aforementioned latency can be achieved. The backhaul latency must be within the range of 5ms in a downlink

transmission so the capacity gain reduction would fall in the range of 20% for the CoMP JT scheme [8].

CHAPTER 3

SIMULATION AND RESULTS

This chapter will present the synchronization requirements for an accurate demodulation process for the CoMP Joint Transmission scheme. The system was tested under the assumption that the two cooperative base stations were assigned to the CoMP JT scheme and there were no frequency offsets among the downlink transmitted signals. All of the simulations here were implemented in MATLAB.

3.1 DATA MODULATION

In wireless communication systems, information such as audio, video, and digital data can be transmitted from one destination to another via electromagnetic radio waves. Data modulation in wireless communication systems occurs when bits are mapped to complex values of I (In Phase) and Q (Quadrature) components of carrier waveforms. There are many modulation techniques used to carry out information by saving the data on the changes of the amplitude and/or the phase of the transmitted signal. A commonly used modulation techniques is Quadrature Phase Shift Keying (QPSK). This technique changes the phase of the carrier waves in order to transmit the data. It uses four distinct phases in order to simultaneously transmit 2 bits per symbol. A QPSK signal can be defined by:

$$s(t) = A_c \cos(2\pi f_c t + \phi(t)); 0 \leq t \leq T \quad (3.1)$$

Where A_c is a constant, f_c is the carrier frequency, T is the duration of the signal, and $\phi(t) = 45, -45, 135, -135$ is the phase shift. Figure 3.1 represents the constellation diagram as well as the real and imaginary part of a complex QPSK symbol. Each point on the constellation diagram is equidistance from the center which is depicted in Figure 3.1. After generating 63 samples of the complex QPSK data sequence, the samples were uploaded to the center bins at a length of 256 points for the IFFT process. The center subcarrier was left empty for the demodulation process at the receiver site. Moreover, the modulation process consisted of shifting the spectrum to the center of the array and converting the frequency

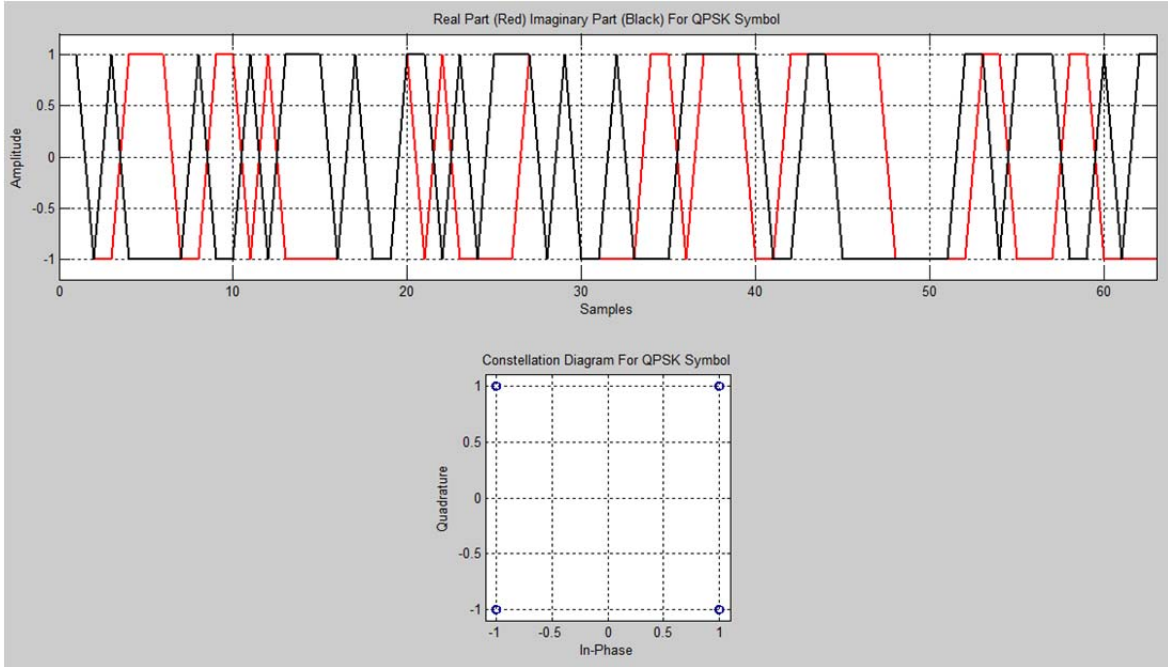


Figure 3.1. Real parts (red line), imaginary parts (black line), and constellation diagram of QPSK symbol.

domain symbol to the time domain signal. Figure 3.2 exhibits the magnitude response, shifting DC component, power spectrum, and time response for the QPSK data.

Another modulation technique commonly used in wireless digital communication is the 16-State Quadrature Amplitude Modulation (16 QAM). The only difference between QPSK and 16 QAM modulation techniques is the fact that the data is not only mapped on the phase, but also on the amplitude of the carrier signals. This scheme is more bandwidth efficient since the modulation rate is implemented on a higher order form. Therefore, it carries more bits per symbol. A 16-QAM signal is defined by Equation 3.2:

$$s(t) = A_m [\cos(2\pi f_c + \phi_m) + \sin(2\pi f_c + \phi_m)]; 0 \leq t \leq T \quad (3.2)$$

Where A_m indicates the amplitude modulation and ϕ_m indicates the phase modulation. While this method offers a faster data rate transmission for the wireless communication systems, it is susceptible to noise and interference. In order to test the receiver under high and low Signal-to-Noise Ratio (SNR), 16 QAM and QPSK symbols were incorporated in the OFDM symbols for the modulation process. Figure 3.3 illustrates the real, imaginary, and the constellation diagram for the 16 QAM symbol. After generating 63 samples of complex 16 QAM data sequences in MATLAB, the samples were uploaded to the center bins with a

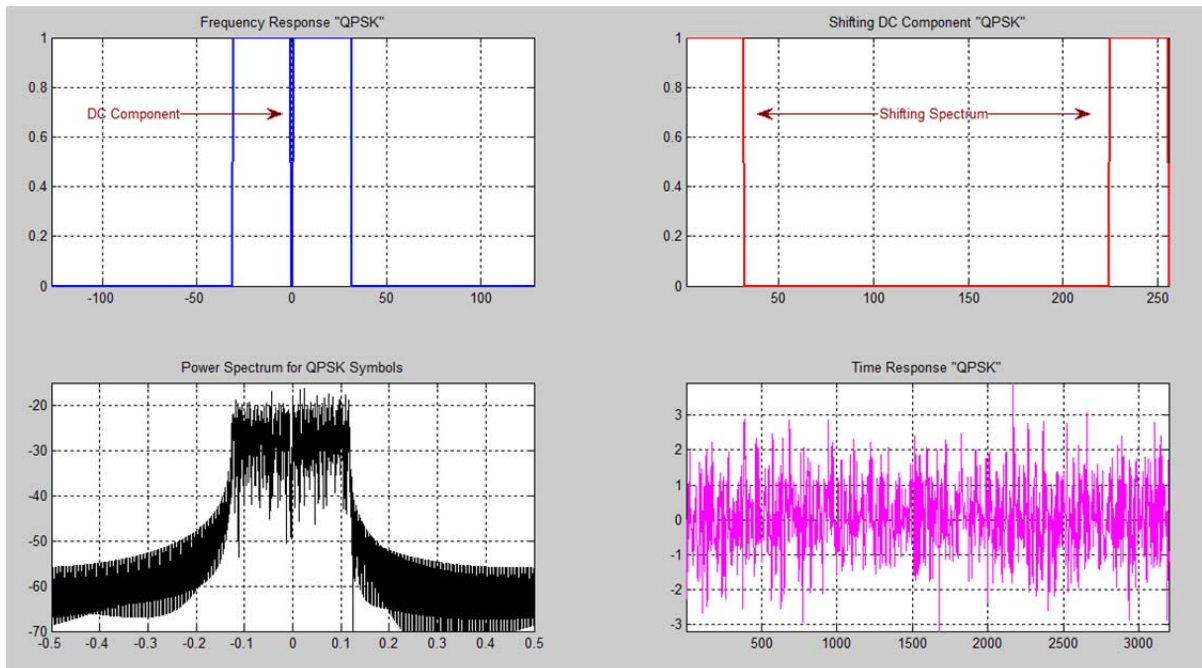


Figure 3.2. Frequency responses, shifting the spectrum, power spectrum, and time response of QPSK symbol.

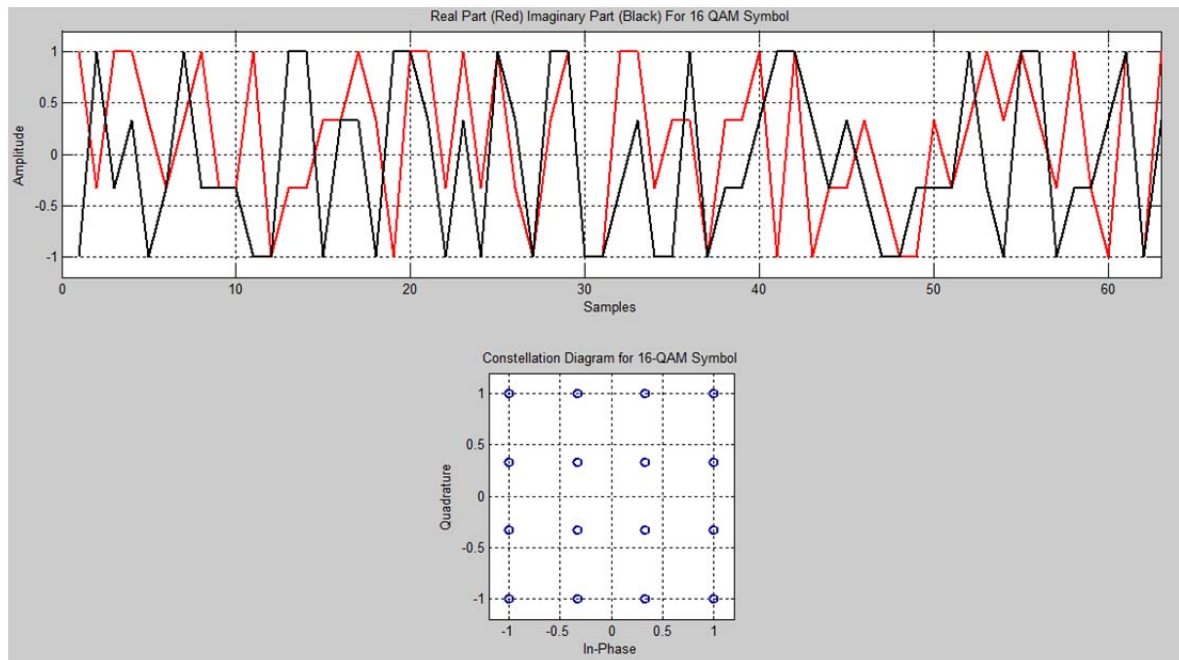


Figure 3.3. Real parts (red line), imaginary parts (black line), and constellation diagram of 16 QAM symbol.

length of 256 points for IFFT process. The center subcarrier was left empty for demodulation process and is illustrated in Figure 3.4:

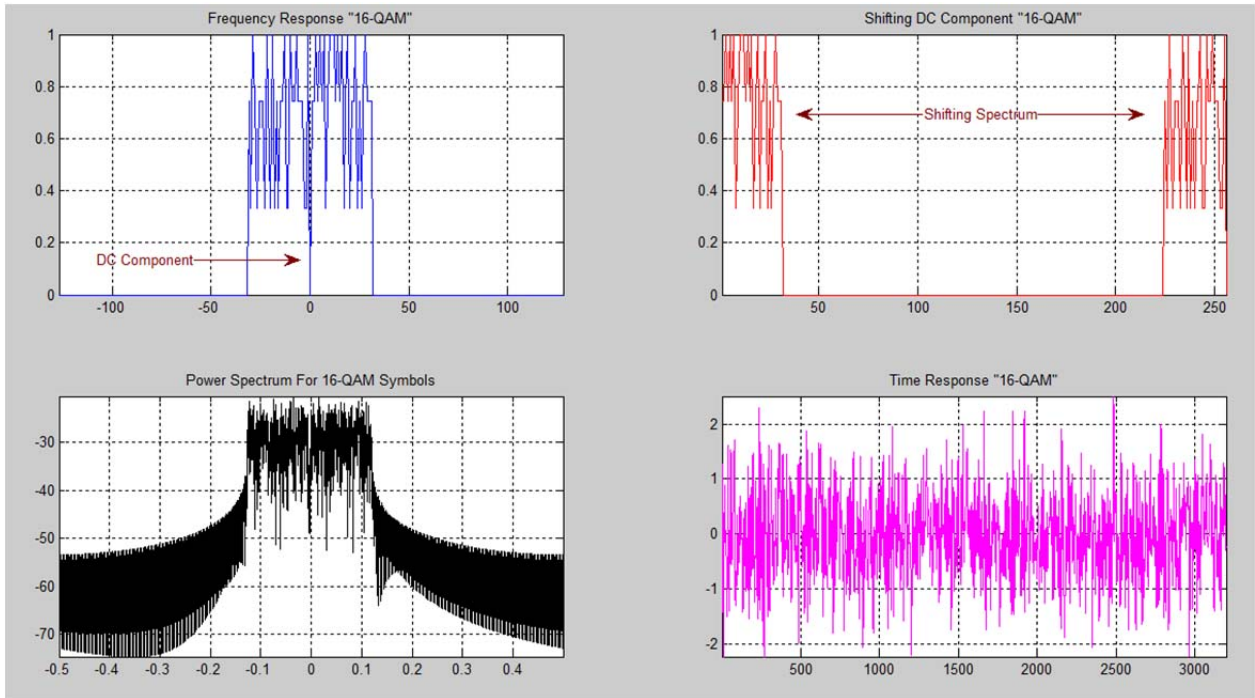


Figure 3.4. Frequency response, shifting the spectrum, power spectrum, and time response of 16 QAM symbol.

The next stage of the modulation process consisted of generating training sequences for the synchronization process. Zadoff-Chu was chosen as the training sequences for the synchronization procedure. The ZC sequence has a low sensitivity to the Doppler frequency shift which makes it a good candidate for frame detection as well as coarse time and frequency offset estimation.

Figure 3.5 demonstrates some of the properties of the ZC sequences which includes the magnitude response, auto-correlation, phase response, and the real and imaginary parts. Equation 2.5 was utilized to generate 63 samples of the ZC sequence (root index of 25). The samples were then uploaded to the center bins at a length of 256 points for the IFFT process. The center subcarrier was left empty for the DC component in order to implement the demodulation process at the receiver site. The next stage of the process involved shifting the spectrum of the symbol to the center of the array. Once the spectrum is shifted, the frequency domain signals are converted to time domain signals. Figure 3.6 illustrates the up sampled

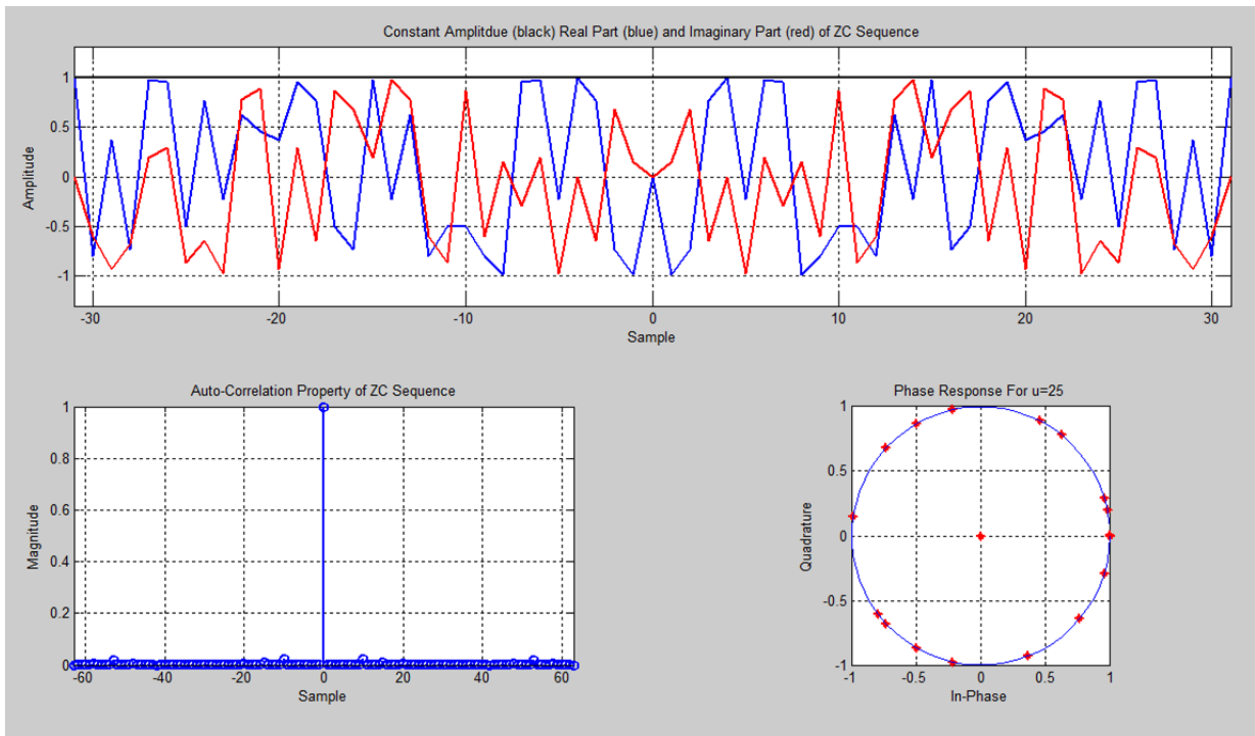


Figure 3.5. Constant Amplitude and Real and Imaginary Parts, Auto-Correlation, Phase of ZC Sequence.

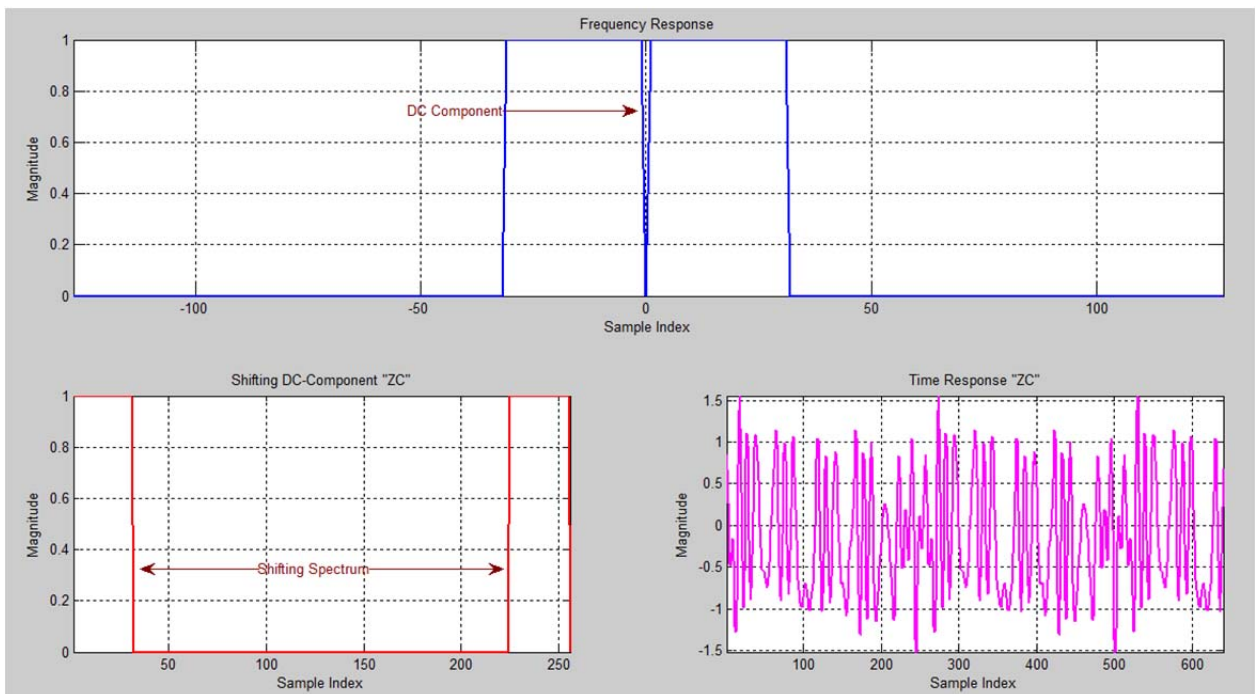


Figure 3.6. Frequency response, shifting the spectrum, and time response of ZC sequence.

sequence (with an empty bin at the center subcarrier), the shifted spectrum of the sequence, and the time response of the ZC sequence.

3.2 OFMD PACKET

The OFDM packet assembly occurred after converting the frequency domain symbols to the time domain signals. Before the OFDM packet assembly, the CP with a length of 64 samples was added to the front of each OFDM symbol in order to prevent the ISI. The length of the CP for training sequences was chosen so that the transmitter places twice the length of the normal CP at the front of the training sequences. The two training sequences were placed right next to each other with no CP in between. This technique is known as Richard Van Nee method [11]. Figure 3.7 illustrates the normal CP versus Richard Van Nee's CP. The advantage of using Richard Van Nee's method is the fact that it makes the sequences more robust against the time delay spread of the channel.

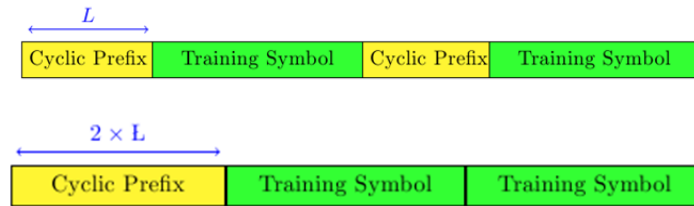


Figure 3.7. Normal CP versus Richard Van Nee's CP.

The OFDM packet assembly for this system consisted of 2 ZC sequences, 10 QPSK symbols, and 10 16-QAM symbols respectively. For this study, QPSK symbols and 16 QAM symbols were utilized for system examination and evaluation. Figure 3.8 illustrates the time response of the OFDM packet-based infrastructure.

In order to model this system in a way that reflects a real world system, signals from transmitter one and two were delayed by 28 and 45 samples respectively and are depicted in Figure 3.9. In OFDM systems there are many sources causing time dispersion in the received signals. Some of these sources consist of: the imperfect timing recovery, sampling jitter due to DAC and ADC, as well as multipath fading channels.

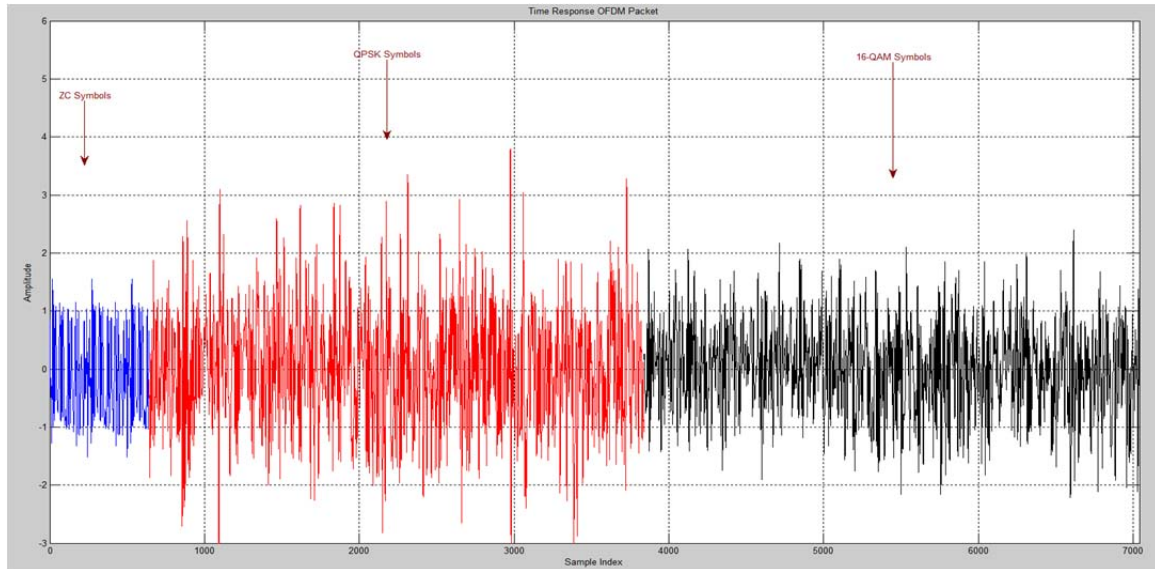


Figure 3.8. OFDM packet.

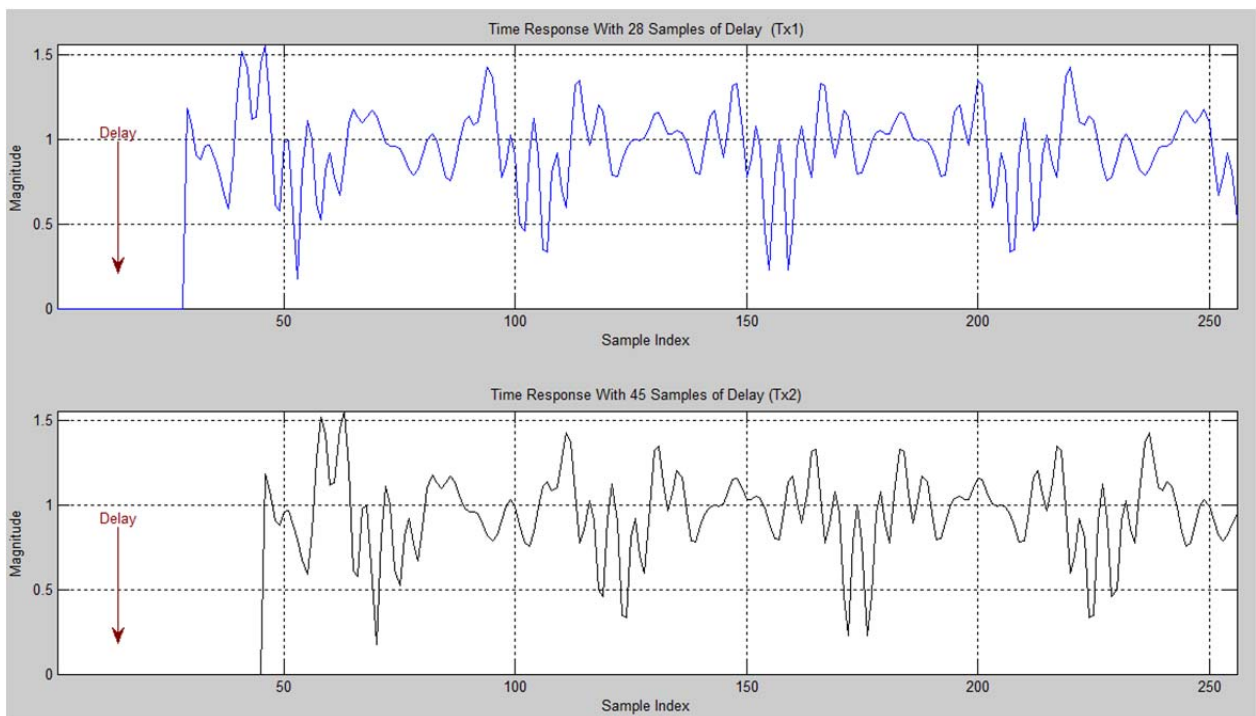


Figure 3.9. Transmitted signals with 28 and 45 samples of delayed from transmitted one and two, accordingly.

3.3 CHANNEL MODEL

Channel modeling is the fundamental phase of designing a wireless communication system. Channel modeling can be described as the relationship between the power for

transmitted signal and the power of the received signal during the transmission process. The goal of channel modeling is to find out how well the wireless communication system performs under the various effects of the channel. The channel model for this simulation process utilized the time-varying multipath fading channel. The time-varying multipath fading channel is defined by Equation 3.3:

$$h[\tau, t] = \sum_{l=0}^{L-1} \alpha_l(t) \delta(\tau - \tau_l) \quad (3.3)$$

Where h , L , α , and τ_l represents the channel impulse response at time instant t , the length of the channel, complex gain, and the delay spread of the channel respectively. The length of the channel for transmitter one consisted of 10 taps (4 of those taps were non-zeroes). The length of the channel for transmitter also consisted of 10 taps (4 of those taps were non-zeroes values). Table 3.1 illustrates the channel parameters used to evaluate the system's robustness. Figure 3.10 depicts the frequency and phase response of the ZC sequences after propagating through the two channels.

Table 3.1. Channel Parameters

	Length of Channel	Number of Non-Zeroes Taps	Channel Impulse Response
Transmitter # 1	10 Taps	4	[1 0 0 j*0.2 0 0 0 0.4 0 0.01]
Transmitter # 2	10 Taps	4	[1 0 0 0.1 0 j*0.3 0 0 0.02 0]

At the receiver site, the two signals were added together inside the channel in order to increase the signal energy. In other words, the signal from transmitter two acts as the constructive interfering signal in order to enhance the single power of the cell edge user. Figure 3.11 shows the magnitude response, time response, and phase response of the two added signals.

Another source of corruption for the received signals was noise. Noise can be generated from many sources, such as electronic components and transmitted interfering signals to name a few. Noise can be modeled as a random sequence or a non-deterministic signal. A random sequence with non-deterministic properties can be described by a probability distribution function. The Additive White Gaussian Noise (AWGN) channel model was used for the simulation process. AWGN adds independent Gaussian noise

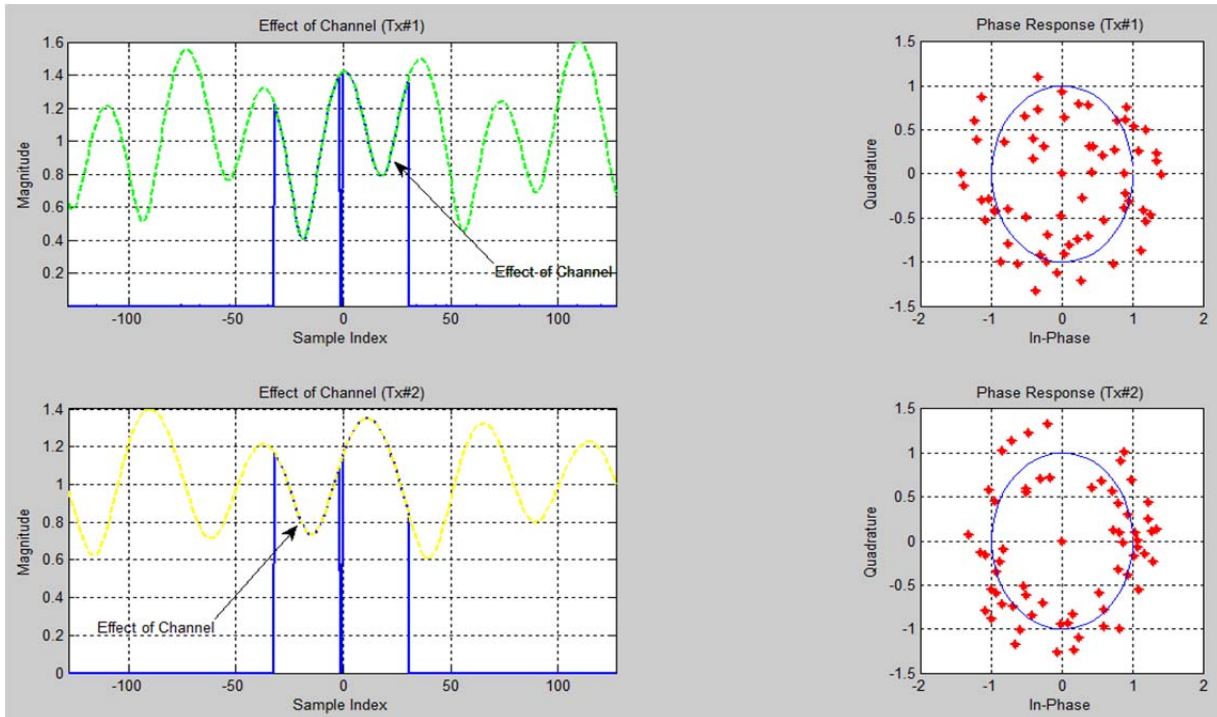


Figure 3.10. Magnitude and phase response of the ZC sequences after propagating through the multipath fading channel for transmitter one and two, respectively.

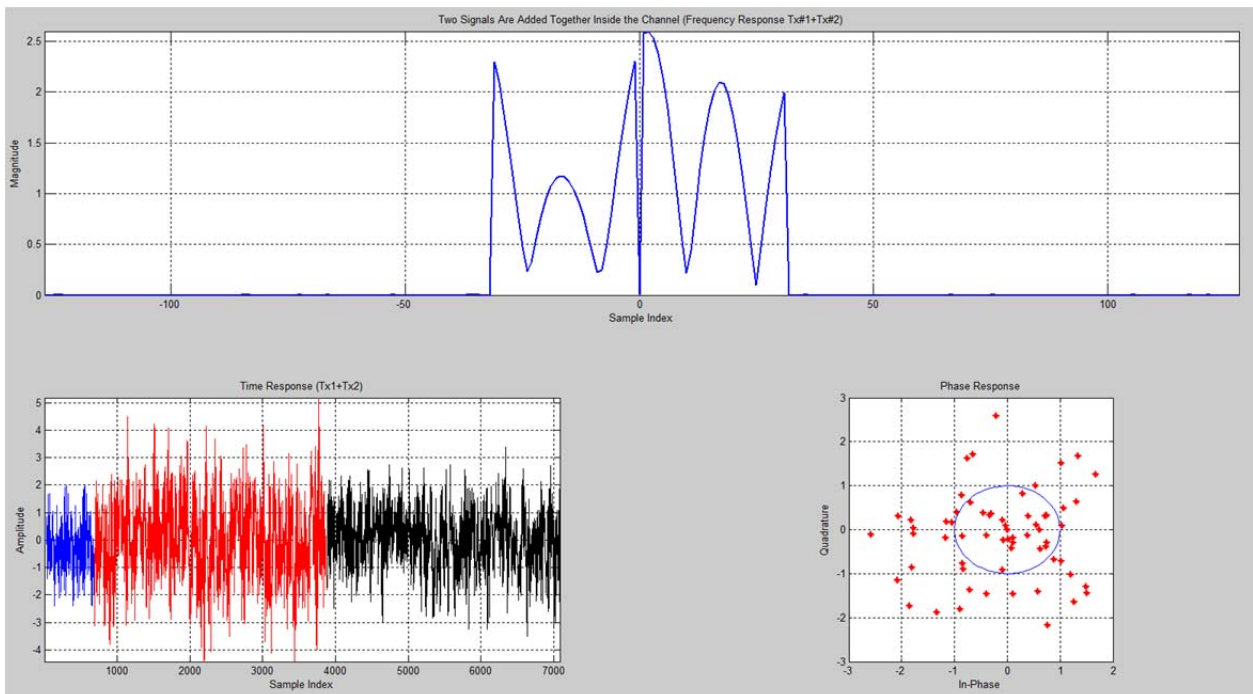


Figure 3.11. Frequency, time, and phase response of the two added signals.

samples to the transmitted signals with uniform power across the frequency band.

Accordingly, the AWGN has a normal distribution in the time domain with an average time domain value of zero [13]. The received signal at the UE can be expressed as follows:

$$y_m = \sum_{i=0}^k h_{mi} x_{mi} + n_m \quad (3.4)$$

Where h_{mi} , x_{mi} and n_m represents the channel impulse response, transmitted signal, and AWGN respectively. In Equation 3.4 k indicates the number of cooperative base stations. The system was evaluated under various values of noise power to derive the effect of the additive noise on the received signals. A normal distributed pseudorandom sequence with respect to the unit Root Mean Square (RMS) was used in MATLAB in order to generate the AWGN. Figure 3.12 illustrates the effect of the AWGN on the received signal. The received signal has a SNR 14 dB.

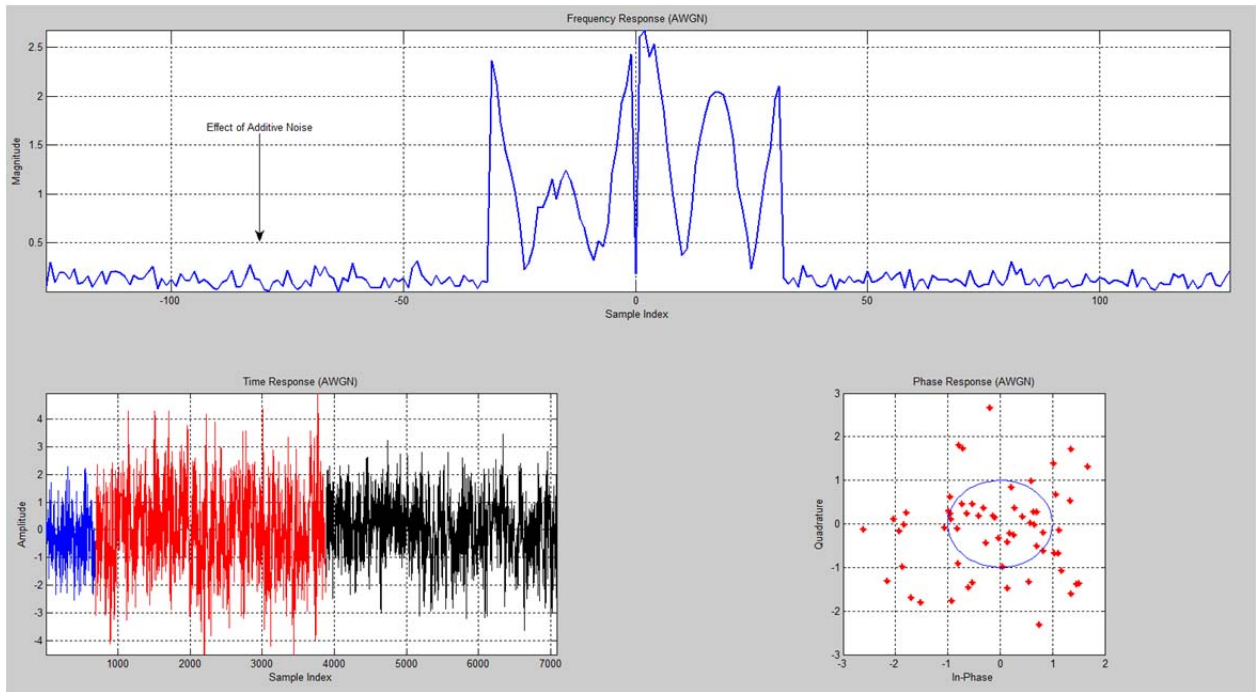


Figure 3.12. The frequency, time, and phase response of the received signal after propagating through an AWGN channel.

3.4 SYNCHRONIZATION PROCESS

In order to model the simulation process in a way that reflects a practical setting, AWGN was also added to the front of the received signal. This ensured that the receiver can detect the signal even with the presence of noise. The Schmidl and Cox algorithm was used as the frame detection process at the receiver. A maximum likelihood detector was utilized

for the integer time offset estimation. The Arbitrary Resampling Interpolator (ARI) with a two nearest neighbor scheme was used to correct the fractional time offset.

3.4.1 AUTOMATIC GAIN CONTROL

The Automatic Gain Control (AGC) in wireless communication systems holds the RMS value of the received signal at a specified level over a wide range of input signal voltage levels. The AGC operates similar to a voltage regulator. A voltage regulator maintains a constant output voltage for a changing input voltage. The classical AGC loop is a time varying system and the system's gains are adjusted according to input signal voltage level. In a logarithmic AGC loop, the feedback loop is solely dependent on the step size μ and is independent of the input variable. The AGC loop is an adaptive feedback loop that consists of a Least Mean Square (LMS) adaptive filter. Figure 3.13 shows an AGC loop consisting of a single variable gain amplifier [14].

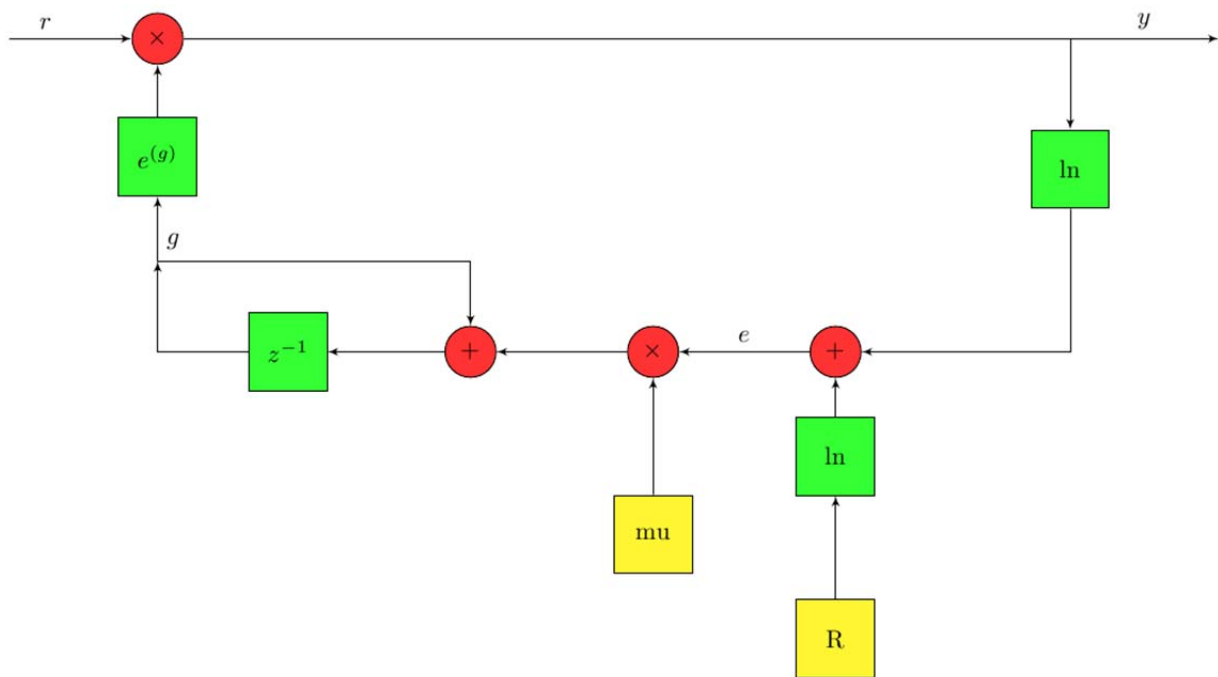


Figure 3.13. Automatic gain control loop. Source: F. J. Harris and G. Smith, “On the design, implementation, and performance of a microprocessor controlled AGC system for a digital receiver,” *IEEE Military Comm. Conf.*, San Diego, CA, 1988, pp 1-55..

In a classical AGC loop, the output signal is the product of the input signal and time varying data dependent weight coefficients of the LMS algorithm. The natural logarithm

function makes the step size μ independent of the input signals making the system unconditionally stable. The output of the feedback loop is compared to the reference value after each loop-iteration is completed and the difference is used to reduce the error of the LMS algorithm. This procedure is shown in Equations 3.5abc:

$$y(n) = e^{g(n)} r(n) \quad (3.5a)$$

$$e(n) = \log(R) - \log(y(n)) \quad (3.5b)$$

$$g(n+1) = g(n) + \mu \times e(n) \quad (3.5c)$$

Where $r(n)$, $y(n)$, $e(n)$, R , μ , and $g(n)$ represent the input signal, output of AGC loop, error signal of the LMS algorithm, reference value, the step size of the LMS algorithm, and gain coefficients [14].

At the receiver site, the AGC algorithm is used to adjust the received signal gain to a reference value R . In Figure 3.14, the first plot illustrates the gain at the output of the AGC loop which is adjusted to the reference value (indicated by the dashed yellow line). The second plot illustrates the error estimation for the LMS algorithm which converges to zero after a certain number of samples. It is also worth noting that the AGC loop did not run during the first 512 samples because it was AWGN. This is due to the fact that the AGC's detector does not recognize the presences of the signal during that time period.

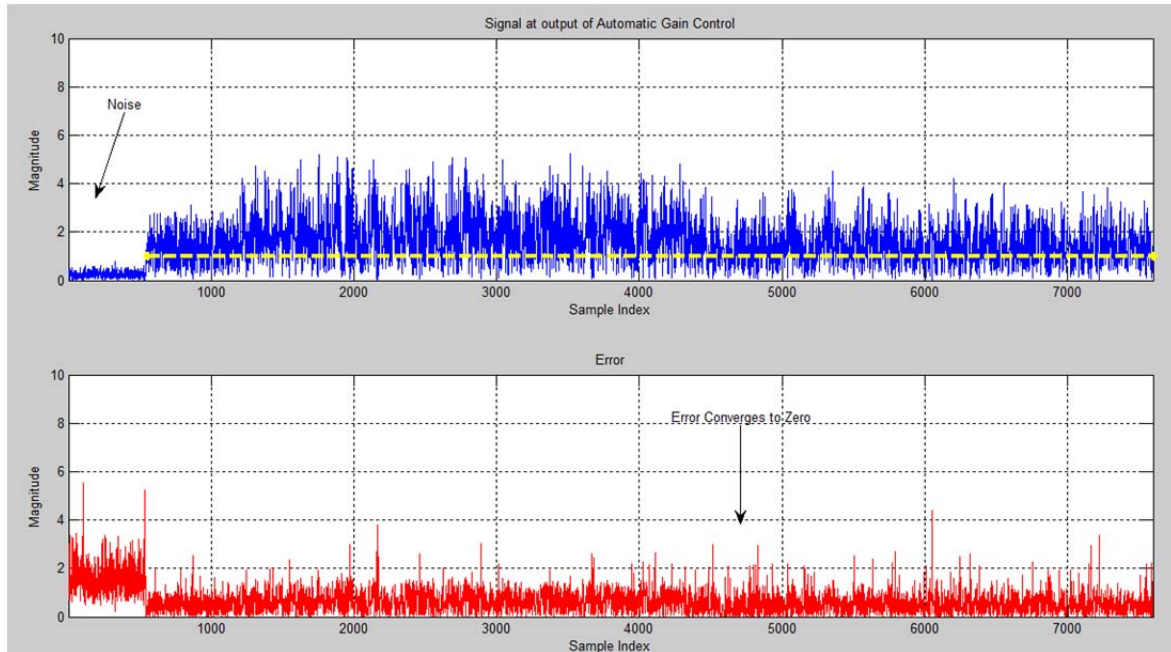


Figure 3.14. Signal level at the output of AGC loop and the error estimation for LMS algorithm.

3.4.2 SCHMIDL AND COX FRAME DETECTION ALGORITHM

The synchronization process for OFDM systems has to determine the symbol timing and will estimate and then correct any time and frequency offsets. Determining the symbol timing for OFDM systems consist of detecting the start of the frames for each OFDM symbol in the presence of the channel and AWGN. There are many algorithms that satisfy the requirements for the frame detection process. One candidate for the frame detection process is the Schmidl and Cox algorithm due to its high efficiency and low computational process. It requires a unique designed preamble with two identical halves. The sequence must satisfy the Constant Amplitude Zero Autocorrelation property for the detection process. Figure 3.15 [15] shows the block diagram for the frame detection and fractional frequency offset estimation for an OFDM system. The first part for the frame detection process is the conjugate of a sample of the first halves of the training sequence multiplied by the corresponding sample of the second halves. The products of each of these pairs of samples will cancel the effect of the channel. At the start of the frame, the magnitude of the sum will have a unit gain since the samples would have the same phase [6]. This operation is known as cross-correlation.

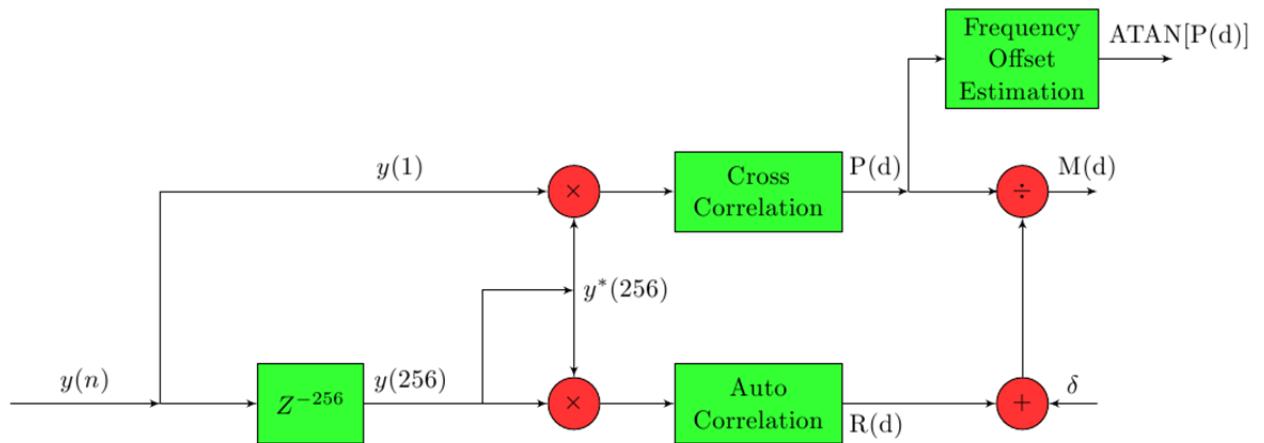


Figure 3.15. Block diagram for frame detection process, time offset estimation, and frequency offset estimation. Source: F. J. Harris and G. Smith, "On the design, implementation, and performance of a microprocessor controlled AGC system for a digital receiver," *IEEE Military Comm. Conf.*, San Diego, CA, 1988, pp 1-55..

In signal processing, the cross-correlation function measures the similarity of the two signals as a function of time with one being delayed. Equation 3.6 shows the cross-correlation function:

$$P(d) = \sum_{m=0}^{L-1} y_{d+m}^* y_{d+m+L} \quad (3.6)$$

Where L and d represent the length of the sequence and the time index of the first sample. The second stage of the frame detection process measures the energy of the received signal by taking the sum of magnitude squared. This operation is known as auto-correlation. The function is shown below in Equation 3.7:

$$R(d) = \sum_{m=0}^{L-1} |y_{d+m+L}|^2 \quad (3.7)$$

Lastly, the magnitude response of the ratio of the cross-correlation function over the auto-correlation function will be the start of the frame. This operation is known as the timing metric estimator. The function is shown in Equation 3.8. The auto-correlation function in the equation below acts as an amplifier to enhance the detection process.

$$M(d) = \frac{|P(d)|}{R(d)+\delta} \quad (3.8)$$

The timing metric function monitors the received signal power and compares it to the threshold δ in order to detect the presence of the OFDM signals. Another advantage to using this algorithm is the fact that the frequency offset estimation is embedded in the algorithm therefore no additional computations are required [7]. By taking the angle of the cross-correlation function the frequency offset can be estimated using Equation 3.9:

$$\theta = \frac{1}{N*2*\pi} \tan^{-1}\{P(d)\} \quad (3.9)$$

Where θ represents the estimated frequency offset. This process is also shown in Figure 3.15. After analyzing the system with different RMS values, the 16 QAM and QPSK modulation techniques for a single transceiver failed at a SNR of 14 dB. Figure 3.16 and 3.17 shows the auto-correlation, cross-correlation process, and the timing metric function for a single transceiver system. The green line in Figure 3.17 indicates the threshold value for the timing metric function which is defined in Equation 3.8. The black line indicates the sample index for which the frame was detected.

Figure 3.18 and 3.19 illustrates the auto-correlation and cross-correlation process, and time metric estimator for a downlink CoMP Joint Transmission system. In Figure 3.17 the frame detection process for a single transceiver was delayed for a channel with a high level

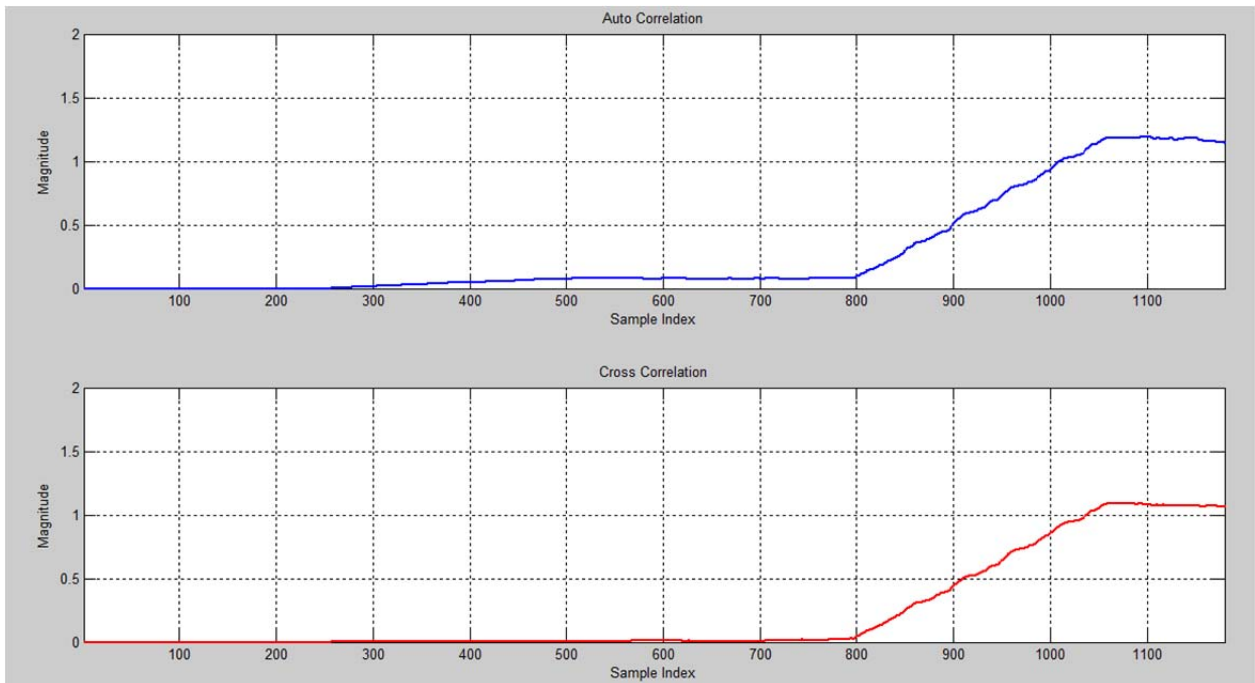


Figure 3.16. Auto-correlation and cross-correlation process for single transmitter and receiver.

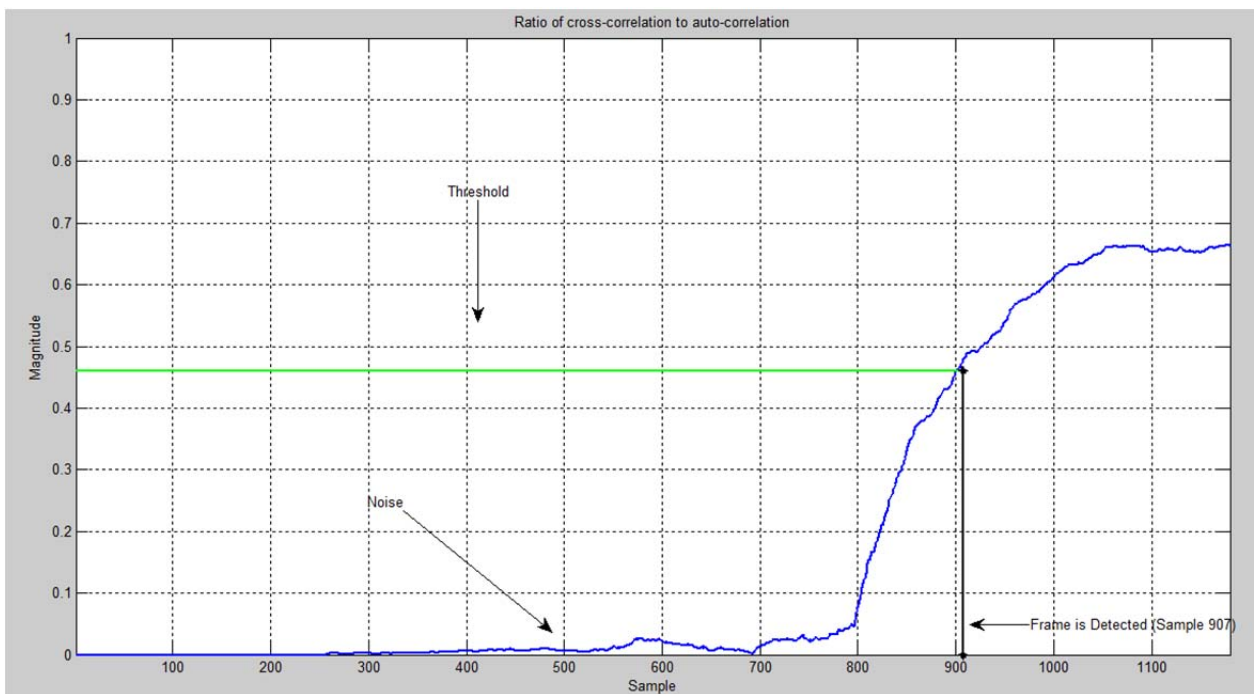


Figure 3.17. Time metric estimator for single transmitter and receiver.

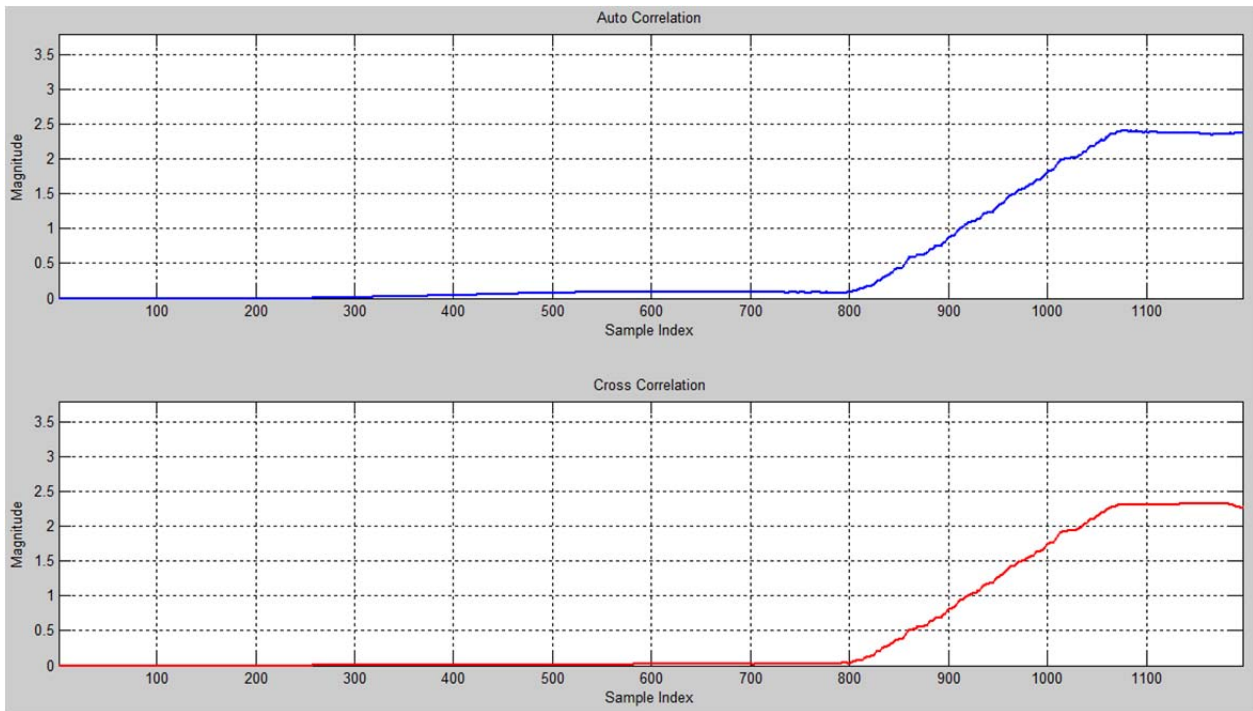


Figure 3.18. Auto-correlation and cross-correlation process for CoMP JT scheme.

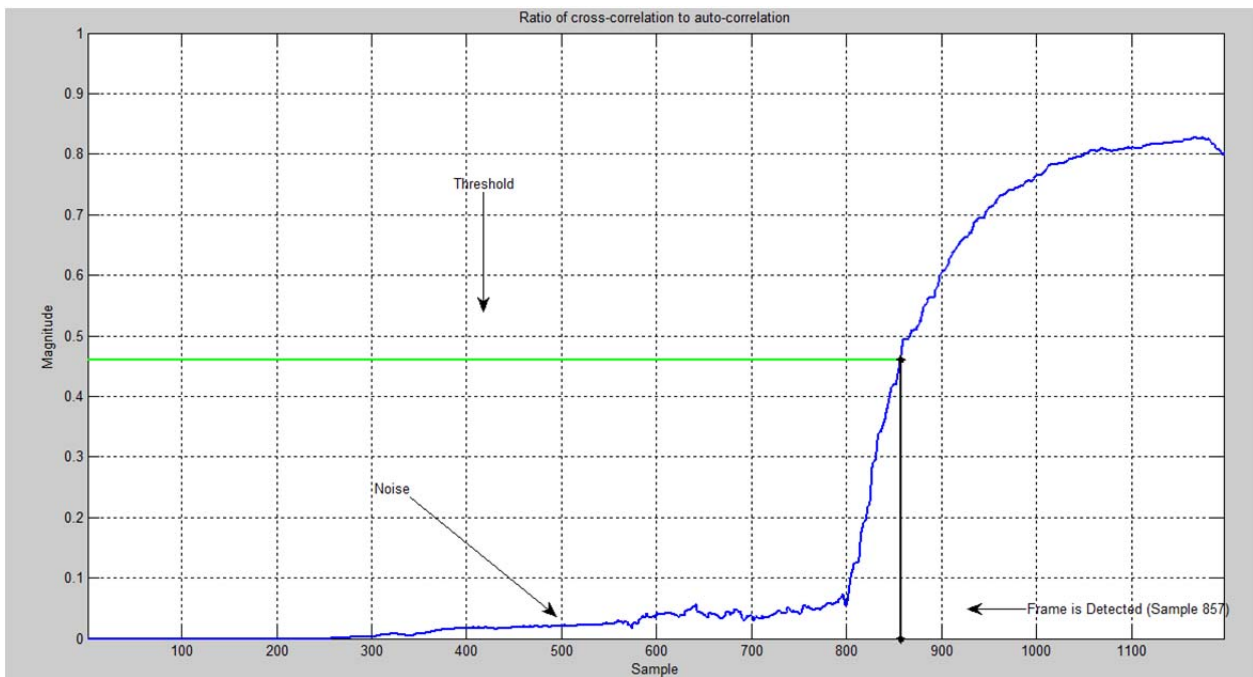


Figure 3.19. Timing metric estimator for CoMP JT scheme.

of noise power. It is clear from the autocorrelation function in Figure 3.18 that the energy of the signal was increased in the CoMP JT scheme compared to the single transmission scenario. In addition, Figure 3.19 confirms that in a CoMP JT scheme the frame detection process for the cell edge UE has been enhanced despite the presence of severe AWGN.

3.4.3 INTEGER TIME OFFSET ESTIMATION

The next phase of the synchronization process is to estimate any time offset among the received signals. This is accomplished without any knowledge of the channel and via the ZC sequence. The method used to find the time offsets is a maximum likelihood detector. The function is illustrated by Equation 3.10:

$$m_k = \underset{k}{\operatorname{argmax}} \left| \sum_{i=0}^{N-1} y[i+m] s_k^*[i] \right|^2 \quad (3.10)$$

Where i is time index, m is the time offset, N is the length of the sequence, $y[i]$ is the received signal at time instant i , and $s_k[i]$ is the replica of ZC sequence with a root index u at time index i [3]. Figure 3.20 depicts the estimated time offsets among the received signals. In Figure 3.20, the red line corresponds to the maximum correlation given there is no time offsets among the received signals. However, the first impulse and the second impulse indicated that there were 28 and 45 samples of delay in the received signals from transmitter one and two.

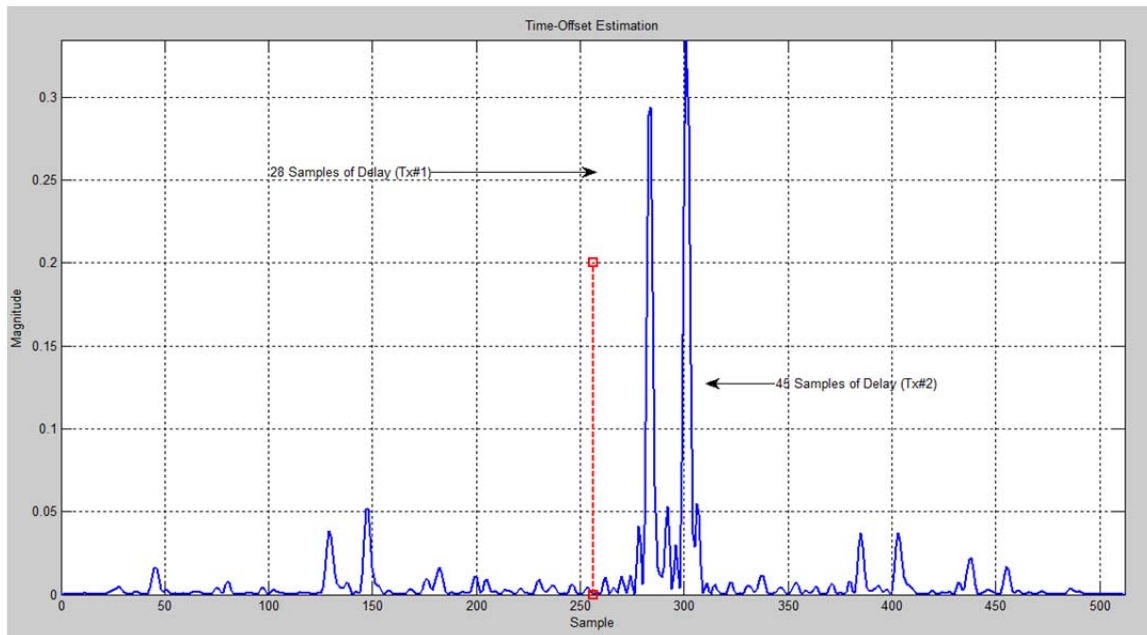


Figure 3.20. Time offset estimation for downlink CoMP JT signals.

3.4.4 FRACTIONAL TIME OFFSET CORRECTION

Fractional time offset can be generated from many sources. Some of these sources include the quantization error of sample value due to the Digital to Analog Converter or Analog to Digital Converter process or a simple up-converting and/or down-converting of the signals causing a mismatch in the sampling time at the receiver. The receiver knows the sampling rate of the received signals, but it does not know the exact time instance of the samples. Some of the effects of the fraction time offset in the received signals includes: a reduction the effectiveness of Cyclic Prefix, induction of ISI, and/or reduction of the SNR. One way to mitigate this dilemma at the receiver site is to utilize an Arbitrary Resampling Interpolator (ARI). For the interpolation process, a P-stage polyphase filter is used to up sample the input signal by P and then down sample the output signal by Q in order to obtain the rational ratio resampling. Normally, the interpolation process calculates the output samples with fractional spacing between the samples of ρT with T being the duration of input sample. If the parameter ρ is a rational ratio of the form P/Q then the precise sample value can be obtained with a polyphase filter. The polyphase filter partitions the input sample intervals into P increments and forms the successive output samples from every Q^{th} port [16]. By increasing the number of the stage in the polyphase filter, the time interval will be small enough to use the output samples. Accordingly, the output samples from the nearest available sample position will form a fine approximation at any arbitrary time location [16]. Another option for correcting fractional time offset is to use an arbitrary resampling interpolator with the two nearest neighbor interpolation scheme. This is achieved by utilizing two P-Stage polyphase filters (where one is the derivate of the other) to estimate the sample value according to the two nearest neighbor sample locations. Figure 3.21 demonstrates the block diagram of the ARI for the two neighbor interpolation scheme [16]. The operation proceeded as follows: a new data sample was shifted into the two 32-path polyphase filter registers in order to compute and generate an output sample point according to the accumulator counter clock. The accumulator is a modulo-32 which means upon overflow of the accumulator will implement the modulo-32 operation. As a result, the counter starts over as a new data point is shifted into the filters. Figure 3.22 illustrates the 63 samples of the signal with and without a fractional time-offset. In the first window of Figure 3.22 the signal with the red line reflects the fractional time-offset whereas the blue line represents the signal

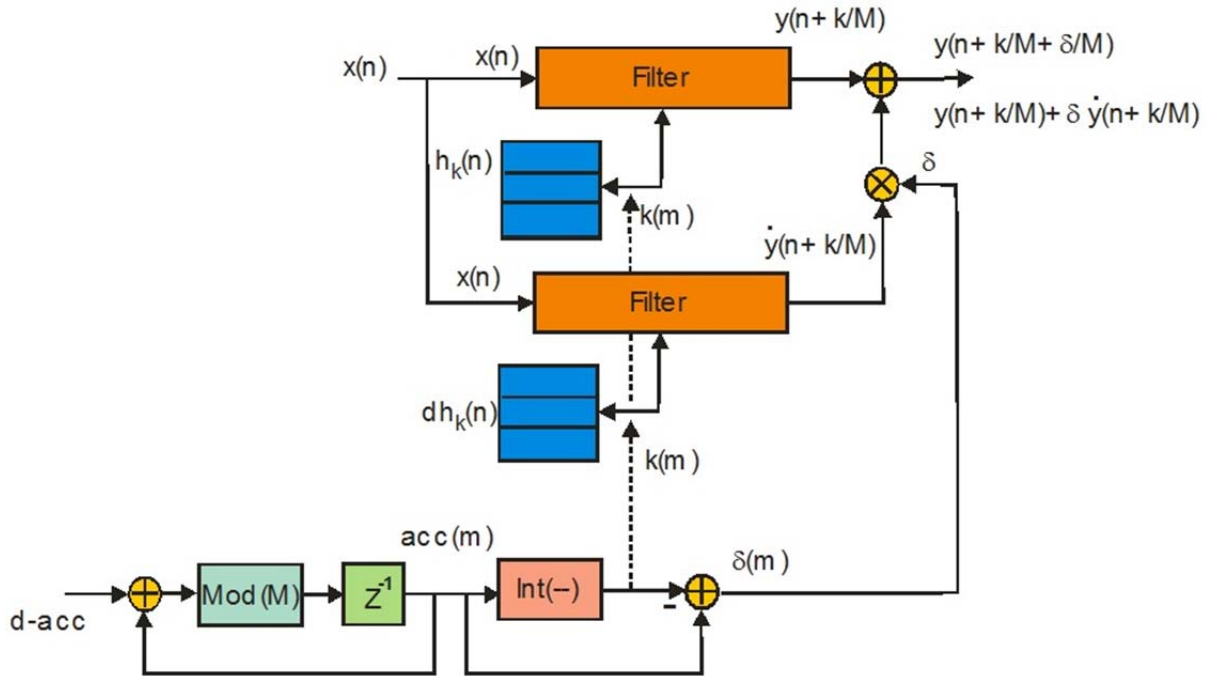


Figure 3.21. Block diagram of arbitrary resampling interpolator with two neighbor interpolation technique. Source: F. J. Harris, *Multirate Signal Processing For Communication Systems*. Upper Saddle River, NJ: Prentice Hall Professional Technical Reference, 2008.

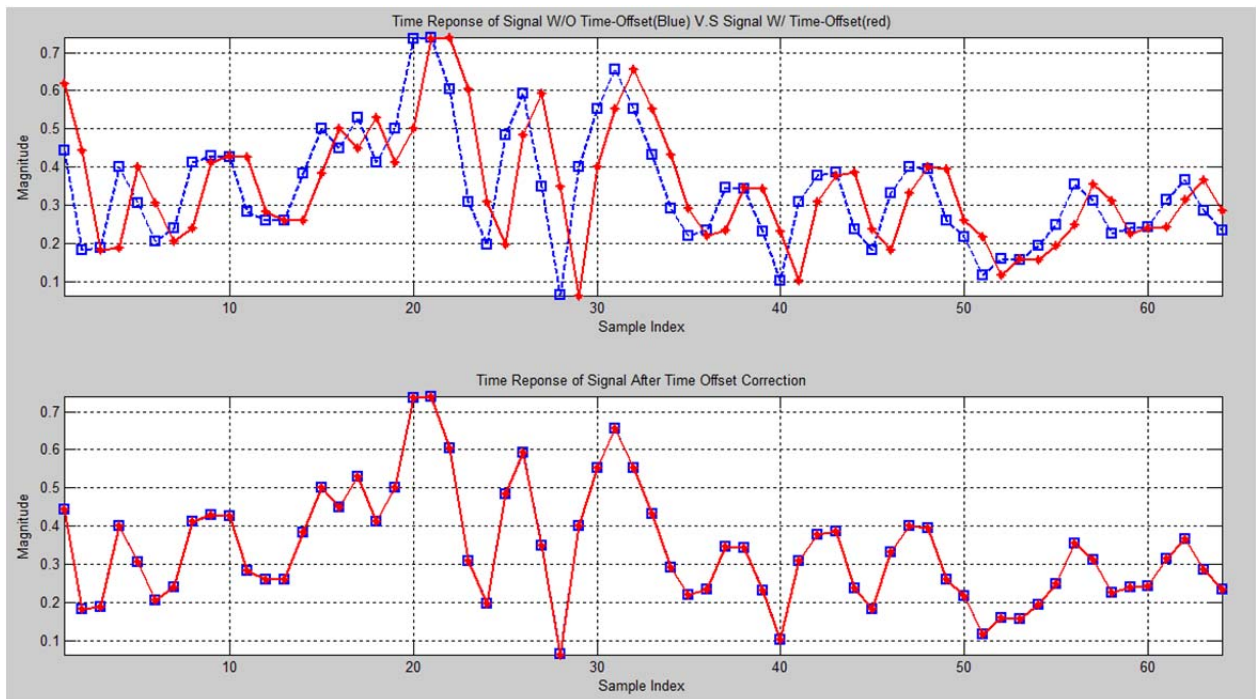


Figure 3.22. Signals at input and output of ARI for two neighbor interpolation technique.

without the fractional time offset. The second window for the same figure shows the signal at the output of ARI once the fractional time offset is corrected. The ARI with the two nearest neighbor interpolation scheme is primarily used to correct fractional time offset for other waveforms. This technique is not typically used in OFDM systems because the fraction time offset is corrected by the channel equalization process.

3.4.5 CHANNEL ESTIMATION

In an OFDM system, a wideband channels is divide into narrowband flat fading sub-channels. Therefore, OFDM symbols will be more robust against frequency-selective multipath fading channels. In data aided synchronization, where the pilot symbols are known at the transmitter and receiver end, the least square (LS) channel equalizer is utilized to remove the distortions caused by the channel. This method requires a low computational process and is efficient as it uses a one-tap decision-direct equalization scheme. This process is represented by Equation 3.11 [17]:

$$\hat{H} = Y/X \quad (3.11)$$

Where \hat{H} is the estimated channel. The red line in top right window for Figure 3.23 shows the estimated channels for the ZC sequence. Channel equalization was achieved after the channel estimation process. The phase response and frequency response of equalized the ZC sequence are also illustrated in the top left window and the bottom window of the same figure.

The next stage of the equalization process consists of equalizing the QPSK and 16 QAM data symbols. These processes are depicted in the Figures 3.24, 3.25.

As previously mentioned, 16 QAM data modulation is more susceptible to channel noise as opposed to QPSK data modulation. Moreover, in the CoMP JT technique, the noise level of the received signals will be doubled for the UE at the cell boundaries. This complication is due to the fact that the transmitted signals propagate through two different channels. As a result, 16 QAM modulation techniques cannot be utilized for data transmission. Figures 3.25 depict the frequency response and the constellation diagram of the 16 QAM symbols (for a downlink CoMP JT scheme with a high level noise power inside the channels). While demodulation process is possible when utilizing the QPSK modulation

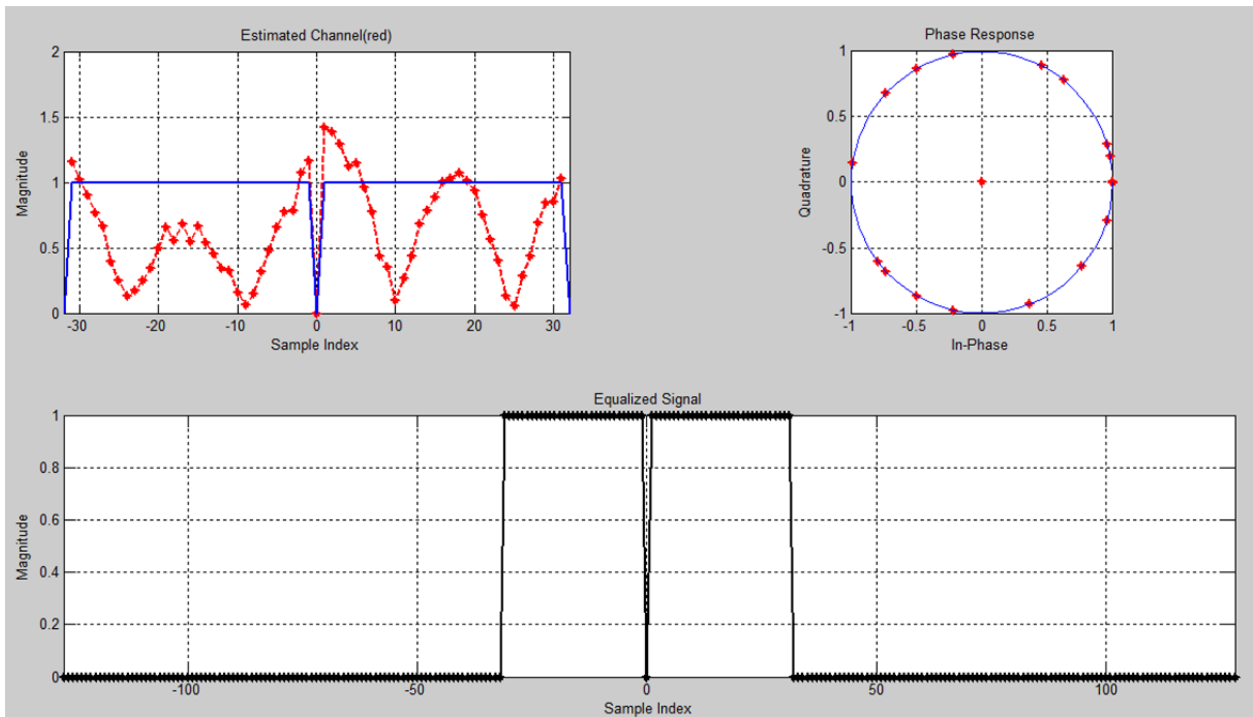


Figure 3.23. Estimated channels via ZC sequence, phase response and frequency response of ZC sequence after equalization process.

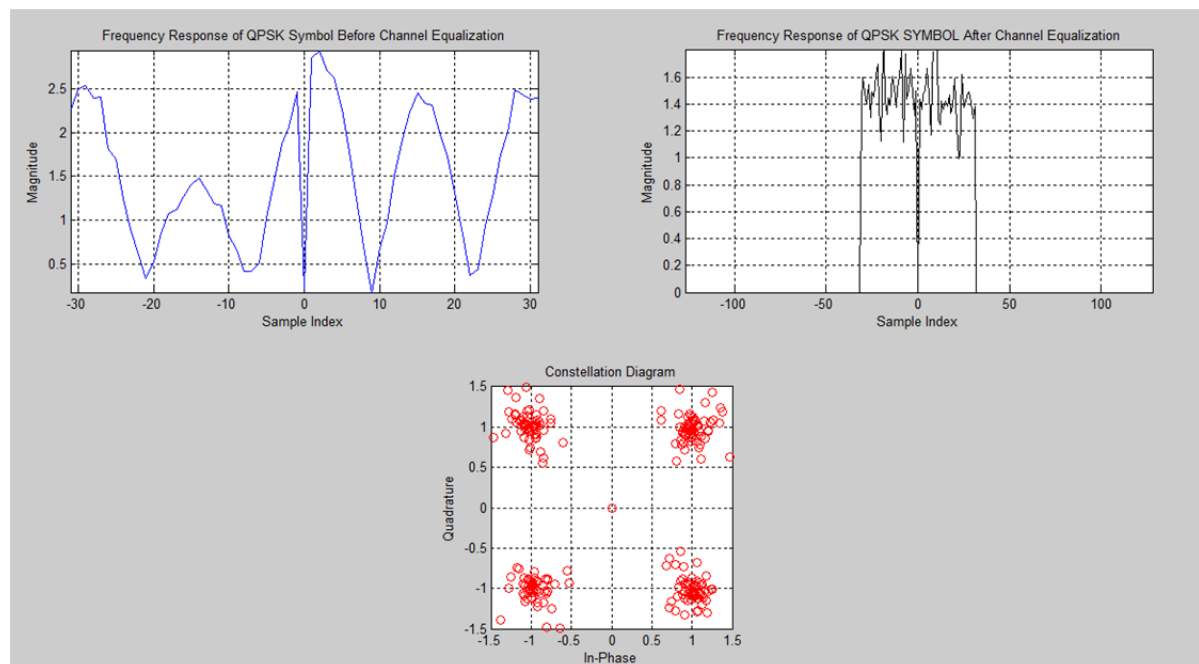


Figure 3.24. Frequency response and constellation diagram of the QPSK Symbols for before and after Channel Equalization process.

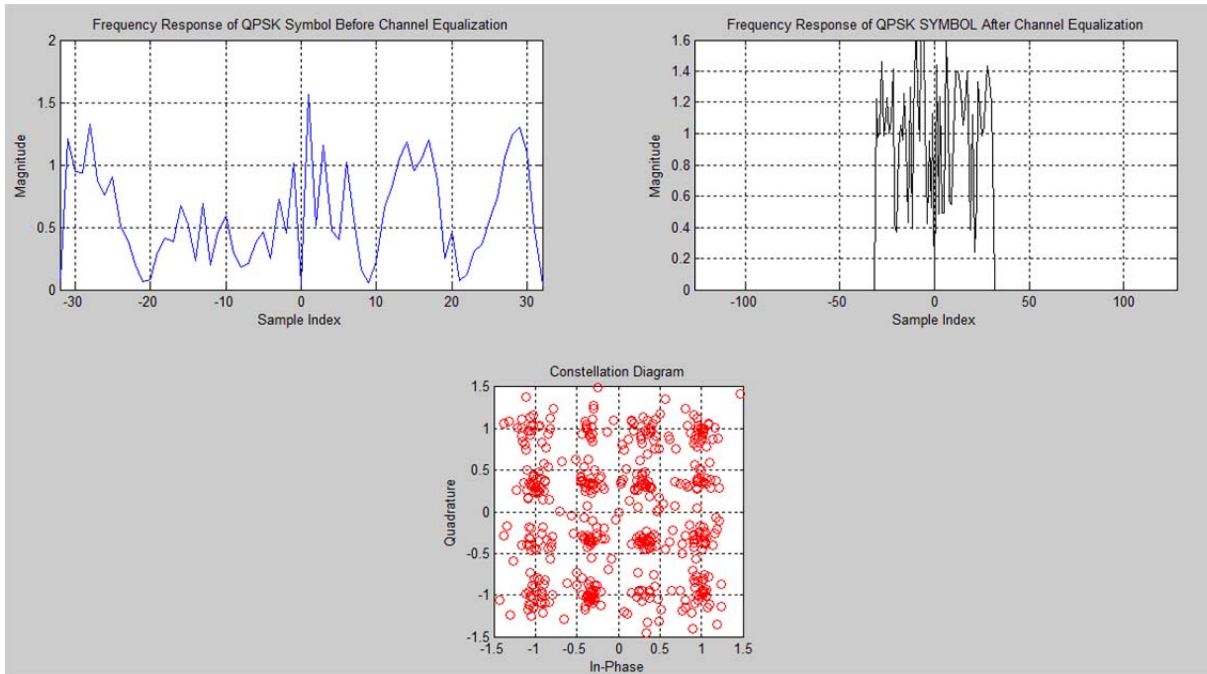


Figure 3.25. Frequency response and constellation diagram of 16-QAM symbol for before and after channel equalization process.

technique, it also requires further equalization. The MATLAB algorithm for the study is presented in the Appendix. All the specifications for the simulation are listed in Table 3.2.

Table 3.2. Simulation Specifications

Specifications	Transmitter 1	Transmitter 2
Training Sequence	Zadoff-Chu Sequence	Zadoff-Chu Sequence
Length of ZC Sequence (Subcarriers)	63	63
Root Index for ZC Sequence	25	25
Number of Pilot Symbols	2	2
Number of Subcarriers for IFFT/FFT	256	256
Length of Cyclic Prefix (Samples)	64	64
Number of QPSK Symbols	10	10
Number of 16 QAM Symbols	10	10
Delays (Samples)	28	45
Length of Multipath Channel	10	10
AWGN RMS_{dB}	-14	-14
SNR of the QPSK Signals	20.7626 (dB)	20.7626 (dB)
SNR of 16 QAM Signals	18.0284 (dB)	18.0284 (dB)

CHAPTER 4

CONCLUSION AND FUTURE WORK

The importance and utility of this research is apparent when analyzing the trends of today's wireless communication market. More consumers are using their mobile phones as a tool for web-browsing or video streaming thus the traffic on the mobile network is increasing and is vulnerable to becoming inundated. As demands for high speed data exchange networks grows, so does the need to enhance the coverage and overall performance cell boards UEs. Several new methods are being investigated to obtain higher data rate transmission. One of these methods is the downlink CoMP with Joint Transmission scheme which can improve the performance as well as cell throughput for cell edge UEs.

This thesis investigated the synchronization requirements for the downlink CoMP JT scheme. While transmitting signals simultaneously from multiple base stations would be ideal as it enhances the synchronization procedures, it also comes at a price. There has to be a tight synchronization among the cooperative base stations via the backhaul link network. If the synchronization process does not consist of a low latency then the received signal will suffer from ISI. There is another method offered in this thesis, for synchronization among the cooperative base stations that produces a more relaxing synchronization process.

Future directions for downlink CoMP JT needs to consider the impact of the Doppler frequency shifts in multipath channels. Specifically transmitted signals with a Doppler frequency shift susceptible to degradation due to ICI. As a result non-coherent demodulation will be implemented at the receiver end. This is due to the fact that the received signals propagate through two different channels with two different Doppler frequency shifts (as seen in Equation 2.15). Consequently, by using the cross-correlation function to estimate the frequency offset, the receiver needs to compensate for 2 frequency offset terms. This operation is illustrated by Equation 4.1:

$$\begin{aligned}
P(d) &= \sum_{n=0}^{N-1} r^*(n+d)r(n) \\
&= \sum_{n=0}^{N-1} a(n+d)[e^{-j\phi_1(n+d)} + e^{-j\phi_2(n+d)}]a(n)[e^{j\phi_1(n)} + e^{j\phi_2(n)}] \\
&= \sum_{n=0}^{N-1} a(n+d)a(n) \begin{bmatrix} e^{j\{\phi_1(n)-\phi_1(n+d)\}} + e^{j\{\phi_2(n)-\phi_1(n+d)\}} \\ + e^{j\{\phi_1(n)-\phi_2(n+d)\}} + e^{j\{\phi_2(n)-\phi_2(n+d)\}} \end{bmatrix} \quad (4.1)
\end{aligned}$$

Where $a(n)$ is the modulated signal and $\phi_1(n)$, $\phi_2(n)$ are the frequency offsets for channel one and two respectively. Because the system is not able to compensate for the second frequency offset the demodulation process cannot proceed. Future work in downlink CoMP Joint Transmissions will require a technique that is able to estimate and compensate for the frequency offsets created by the Doppler frequency shifts in the multipath fading channels.

REFERENCES

- [1] S. Parkvall et al., "LTE-Advanced – evolving LTE towards IMT-Advanced," *68th IEEE Vehicular Technology Conference*, 2008, pp. 1-5.
- [2] P. Marsch and G. P. Fettweis, *Coordinated Multi-Point in Mobile Communications From Theory To Practice*. Cambridge, NY: Cambridge University Press, 2011.
- [3] E.M. Silva et al., "Cell search in long term evolution systems: primary and secondary synchronization," *Circuits and Systems (LASCAS)*, Playa del Carmen, Mexico, 2012, pp. 1-4.
- [4] E. Dahlman et al., *4G LTE/LTE-Advanced for Mobile Broadband*. Burlington, MA: Academic Press, 2011.
- [5] C. E. M. Silva, F. J. Harris, and G. J. Dolecek, "Synchronization algorithm based on a weighted CAZAC preambles for OFDM systems," *Communications and Information Technology (ISCIT)*, 2013, pp. 192-197.
- [6] T. M. Schmidl and D. C. Cox, "Robust frequency and timing synchronization for OFDM," *IEEE. Comm.*, vol. 45, pp. 1613-1521, Dec. 1997.
- [7] S. Sesla and I. Toufik, *LTE - The UMTS Long Term Evolution From Theory To Practice*. West Sussex, UK: John Wiley & Sons, 2011.
- [8] K. Manolakis et al., "Analytical models for channel aging and synchronization errors for base station cooperation," *European Signal Processing Conference (EUSIPCO)*, Marrakech, Morocco, 2013, pp. 1-5.
- [9] V. Jungnickel et al., "Synchronization of cooperative base stations," *IEEE International Symposium Wireless Communication Systems*, Munich, Germany, 2008, pp. 329-334.
- [10] F. Harris, private communication, Jan., 2014.
- [11] A. M. Hamza and J. W. Mark, "A timing synchronization scheme in coordinated base-stations cooperative communications," *Wireless Communication & Signal Processing (WCSP)*, 2012, pp. 1-6.
- [12] R. Irmer et al., "Coordinated multipoint: concepts, performance, and field trial results," *IEEE. Comm. Magazine*, vol. 49, pp. 102-111, Feb. 2011.
- [13] S. N. K. Marwat, "LTE channel modelling for system level simulations," M.S. thesis, Dept. Comm. Netwo., Bremen. Univ., Bremen, Germany, 2011.
- [14] F. J. Harris and G. Smith, "On the design, implementation, and performance of a microprocessor controlled AGC system for a digital receiver," *IEEE Military Communications Conference*, San Diego, CA, 1988, pp 1-55.
- [15] F. J. Harris, "Orthogonal frequency division multiplexing (OFDM)," Presented at Department of Electrical Engineering, San Diego State University, San Diego, CA, 2008.

- [16] F. J. Harris, *Multirate Signal Processing For Communication Systems*. Upper Saddle River, NJ: Prentice Hall Professional Technical Reference, 2008.
- [17] S. Coleri et al., "Channel Estimation Techniques Based on Pilot Arrangement in OFDM Systems," *IEEE Trans. Broadcasting*, vol. 48, pp. 223-229, Sep. 2002.

APPENDIX
MATLAB SCRIPTS

```

%% Clearing & Closing all Functions and Figures
close all
clear all
clc
%% Modulation Process for ZC-Sequence
N          = 64;           % # of Used Bins
UPS        = 4;           % Up Sampling Factor
A          = 8*UPS;        % Scaling Factor
FFT=(2/N)log2(N)
L          = UPS*N;        % # of Bins for IFFT
T          = ((-(N/2-1):N/2-1)+L/2); % Center Bin for DC
Component
u          = 25;           % Root Index
% ===== %
parfor n = 0:N-2
    ZC(n+1) = exp(-j*(pi*u*n*(n+1))/(N-1)); % Generating
    Zadoff_Chui seq.
end
% ===== %
ZC_DC      = ZC;
ZC_DC(N/2) = 0;
% ===== %
ZC_SYM     = zeros(1,L); % Storage
zc_sig     = [];         % Storage
a          = 0;           % Counter
s          = 2;           % Number of ZC Symbols
% ===== %
for n = 1:s
    ZC_SYM(T) = ZC; % Uploading ZC to the
    % Center Bins
    ZC_SYM(L/2) = 0; % Adding DC to Center
    % Bin
    ZC_SH      = fftshift(ZC_SYM); % Shifting DC
    Component
    % ===== %
    zc          = A*ifft(ZC_SH); % Generating Time
    % domain Signal
    zc_sig      = [zc_sig zc]; % Generating OFDM ZC
    packets
    a          = a + 1;
    % ===== %
    if a == s
        zc_cp      = zc(1+L/2:end); % Generating CP
        zc_packet   = [zc_cp zc_sig]; % Adding CP
    end
end
% ===== %
figure(14)
subplot(121)
plot(-(N-2)/2:(N-2)/2,real(ZC_DC),'b','linewidth',1.5)
hold on
plot(-(N-2)/2:(N-2)/2,imag(ZC_DC),'r','linewidth',1.5)
plot(-(N-2)/2:(N-2)/2,abs(ZC_DC),'--k','linewidth',2)
hold off
title('Real Part (blue), Imaginary Part (red) and Magnitude (black) of
Zadoff-Chui sequence')

```

```

xlabel('Sample');ylabel('Amplitude');grid on
axis([- (N-2)/2 (N-2)/2 -1.3 1.3])
% ===== %
subplot(122)
plot(ZC_DC,'r','linewidth',2)
hold on
plot(exp(1i*2*pi*1/(N-1)*(1:N-1)), 'linewidth',1)
hold off
title('Phase Response');
xlabel('In-Phase');ylabel('Quadrature')
axis('square');grid on
pause
% ===== %
figure(16)
subplot(211)
plot(-(L/2-1):L/2,abs(ZC_SYM), 'b', 'linewidth',2)
grid on
axis('tight')
title('Frequency Response')
xlabel('Sample Index');ylabel('Magnitude')
% ===== %
subplot(223)
plot(abs(ZC_SH), 'r', 'linewidth',2)
grid on
axis('tight')
title('Shift in the Spectrum "ZC"')
xlabel('Sample Index');ylabel('Magnitude')
% ===== %
subplot(224)
plot(real(zc_packet), 'm', 'linewidth',1.5)
grid on
axis('tight')
title('Time Response "ZC"')
xlabel('Sample Index');ylabel('Magnitude')
pause
%% Transmitter # 1
tx1_sig = [zc_packet]; % OFDM Packets
smp1 = 28; % Delay for Tx#1
delay1 = zeros(1,smp1); % Generating Delay
(Tx#1)
tx1_dly = [delay1 tx1_sig]; % Txed Signal with L
Samples of Delay (Tx#1)
% ===== %
L_ZC = length(zc_packet);
%% Transmitter # 2
smp2 = 45; % Delay for Tx#2
delay2 = zeros(1,smp2); % Generating Delay
(Tx#2)
tx2_dly = [delay2 tx1_sig]; % Txed Signal With K
Samples of Delay (Tx#2)
% ===== %
figure(20)
plot(1:L_ZC,real(tx1_sig(1:L_ZC)))
axis([0 length(tx1_sig)+1 -3 6])
grid on
xlabel('Sample Index');ylabel('Amplitude')

```

```

        title('Time Response OFDM Packet')
        pause
% ===== %
figure(21)
    subplot(211)
    plot(abs(tx1_dly(1:L)), 'b')
    grid on
    axis('tight')
    xlabel('Sample Index'); ylabel('Magnitude')
    title('Time Response With 28 Samples of Delay (Tx1)')
% ===== %
    subplot(212)
    plot(abs(tx2_dly(1:L)), 'k')
    grid on
    axis('tight')
    xlabel('Sample Index'); ylabel('Magnitude')
    title('Time Response With 45 Samples of Delay (Tx2)')
    pause
%% Channel (Tx#1)
ch_1 = [1 0 0 j*0.2 0 0 0 0.4 0 0.01]; % Length of Channel
tx1_ch = filter(ch_1,1,tx1_dly); % Convolver Channel
with Signal
% ===== %
l_zc_cp = length(zc_cp);
sc1 = tx1_ch(1+smp1:L_ZC);
sc1 = sc1(1+l_zc_cp:l_zc_cp+L);
SC1 = 1/A*fftshift(fft(sc1,L));
SCF1 = SC1(T);
%% Channel (Tx#2)
ch_2 = [1 0 0 0.1 0 j*0.3 0 0 0.02 0]; % Length of channel L
tx2_ch = filter(ch_2,1,tx2_dly); % Convolver channel
with signal
% ===== %
sc2 = tx2_ch(1+smp2:L_ZC);
sc2 = sc2(1+l_zc_cp:l_zc_cp+L);
SC2 = 1/A*fftshift(fft(sc2,L));
SCF2 = SC2(T);
% ===== %
    figure(34)
    subplot(221)
    plot((-0.5:1/L:0.5-1/L)*L,abs(SC1), 'b', 'linewidth',2)
    title('Effect of Channel (Tx#1)')
    xlabel('Sample Index'); ylabel('Magnitude'); grid on
    axis('tight')
% ===== %
    subplot(222)
    plot(SCF1, '*r', 'linewidth',1.5)
    hold on
    plot(exp(1i*2*pi*1/(N-1)*(1:N-1)), 'linewidth',1)
    hold off
    title('Phase Response (Tx#1)');
    xlabel('In-Phase'); ylabel('Quadrature')
    grid on
    axis('square')
% ===== %
    subplot(223)

```

```

plot((-0.5:1/L:0.5-1/L)*L,abs(SC2),'b','linewidth',2)
title('Effect of Channel (Tx#1)')
xlabel('Sample Index');ylabel('Magnitude');grid on
axis('tight')
title('Effect of Channel (Tx#2)')
xlabel('Sample Index');ylabel('Magnitude')
grid on
axis('tight')
% ===== %
subplot(224)
plot(SCF2,'*r','linewidth',1.5)
hold on
plot(exp(1i*2*pi*1/(N-1)*(1:N-1)),'linewidth',1)
hold off
title('Phase Response (Tx#2)');
xlabel('In-Phase');ylabel('Quadrature')
grid on
axis('square')
pause
%% Frequency Offset (Tx#1)
delta_1 = 0.00;
% ===== %
fo_1 = exp(1i*2*pi*delta_1/L*(1:length(tx1_ch))); % Generating Freq
Offset
tx1_fo = fo_1.*tx1_ch; % Adding Freq offset
%% Frequency Offset (Tx#2)
delta_2 = 0.000;
% ===== %
fo_2 = exp(1i*2*pi*delta_2/L*(1:length(tx2_ch))); % Generating Freq
Offset
tx2_fo = fo_2.*tx2_ch; % Adding Freq Offset
% ===== %
%% Adding Two Signal (At The RX Side)
tot_sig = [tx1_fo zeros(1,smp2-smp1)]+tx2_fo; % TX1+TX2 (Adding the
signals inside the channel)
% ===== %
sf3 = tot_sig(1:L_ZC);
sf3 = sf3(1+l_zc_cp:l_zc_cp+L);
SF3 = 1/A*fftshift(fft(sf3));
SFF3 = SF3(T);
% ===== %
figure(39)
subplot(211)
plot(-L/2+1:L/2,abs(SF3),'b','linewidth',1.5)
title('Two Signals Are Added Together Inside the Channel (Frequency
Response Tx#1+Tx#2)')
xlabel('Sample Index');ylabel('Magnitude');grid on
axis('tight')
% ===== %
subplot(223)
plot(1:L_ZC+smp2,real(tot_sig(1:L_ZC+smp2)))
title('Time Response (Tx1+Tx2)')
grid on
xlabel('Sample Index');ylabel('Amplitude');grid on
axis('tight')
% ===== %

```

```

subplot(224)
plot(SFF3, '*r', 'linewidth', 1.5)
hold on
plot(exp(1i*2*pi*1/(N-1)*(1:N-1)), 'linewidth', 1)
hold off
title('Phase Response');
xlabel('In-Phase'); ylabel('Quadrature')
grid on
axis('square')
pause

%% Adding Noise to The Signal **20*log10(RMS)** (Noise Level (RMS) With
Respect To Unity)
RMS = 0.199526231; % -14dB
awgn1 = RMS*(randn(1,length(tot_sig))+1i*randn(1,length(tot_sig))); %
Generating AWGN
awgn4 = RMS*(randn(1,2*L)+1i*randn(1,2*L)); % Generating AWGN
L_AWGN = length(awgn4); % length of AWGN
% ===== %
rx = tot_sig+awgn1; % (W/O Noise)CH+FO+AWGN
rn = [awgn4 rx]; % CH+FO+AWGN
% ===== %
sn = rx(1:L_ZC);
sn = sn(1+l_zc_cp:l_zc_cp+L);
SN = 1/A*fftshift(fft(sn));
SNF = SN(T);
% ===== %
figure(41)
subplot(211)
plot(-L/2+1:L/2,abs(SN), 'b', 'linewidth', 1.5)
title('Frequency Response (AWGN)')
xlabel('Sample Index'); ylabel('Magnitude'); grid on
axis('tight')
% ===== %
subplot(223)
plot(1:L_ZC+smp2,real(rx(1:L_ZC+smp2)))
axis('tight')
xlabel('Sample Index'); ylabel('Amplitude'); grid on
title('Time Response (AWGN)')
% ===== %
subplot(224)
plot(SNF, '*r', 'linewidth', 1.5)
hold on
plot(exp(1i*2*pi*1/(N-1)*(1:N-1)), 'linewidth', 1)
hold off
title('Phase Response (AWGN)');
xlabel('In-Phase'); ylabel('Quadrature')
grid on
axis('square')
pause

%% AGC
L_RN = length(rn);
% ===== %
yg_sv = zeros(1,L_RN); % Storage
A = 1; % Reference value5
mu = 0.000003; % Step Size for LMS Alg.
wts = 0.001;

```

```

for n = 1:L_RN
    y_g      = exp(wts)*rn(n);           % Output of AGC
    yg_sv(n) = y_g;                     % Saving the output
    e(n)      = log(A)-log(abs(y_g));    % Adjusting the gain for
LMS
    wts      = wts+mu*e(n);             % Optimizing the weight
coeffs of LMS Alg.
end
% ===== %
figure(43)
    subplot(211)
    plot(abs(yg_sv))
    grid on
    title('Signal at output of Automatic Gain Control')
    xlabel('Sample Index');ylabel('Magnitude')
    axis([1 length(rn) 0 10])
    % ===== %
    subplot(212)
    plot(abs(e), 'r')
    grid on
    title('Error')
    xlabel('Sample Index');ylabel('Magnitude')
    axis([1 length(rn) 0 10])
    pause
%% Receiver (Schmidl & Cox Alg) & AGC
dly      = zeros(1,L+1);               % Storage for delay
cross_set = zeros(1,L);                % Storage
auto_set  = zeros(1,L);                % Storage
th        = .46;                       % Threshold
% ===== %
for n = 1:L_RN
    dly      = [yg_sv(n) dly(1:L+1)];
    cross     = dly(1)*conj(dly(L+1));   % Cross-correlation
    auto      = dly(L+1)*conj(dly(L+1)); % Auto-correlation
    cross_set = [cross cross_set(1:L-1)]; % Saving and Flipping
    auto_set  = [auto auto_set(1:L-1)];   %
    avg_crs(n) = sum(cross_set)/(L);      % Averaging Filter for
cross-correlation
    avg_at(n)  = sum(auto_set)/(L);      % Averaging Filter for
auto-correlation
    % ===== %
    ratio(n)   = avg_crs(n)/(avg_at(n)+th); % ratio of cross/auto
correlation
end
% ===== %
L_R      = L_AWGN+smp2+L_ZC;
str_frm  = 1+L_AWGN+l_zc_cp+L-40;
% ===== %
figure(45)
    subplot(211)
    plot(abs(avg_at), 'linewidth', 1.5)
    title('Auto Correlation');grid on
    xlabel('Sample Index');ylabel('Magnitude');
    axis([1 L_R 0 3.8])
    % ===== %
    subplot(212)

```

```

    plot(abs(avg_crs), 'r', 'linewidth', 1.5)
    title('Cross Correlation'); grid on
    xlabel('Sample Index'); ylabel('Magnitude')
    axis([1 L_R 0 3.8])
    pause
% ===== %
    figure(46)
    plot(abs(ratio), 'linewidth', 1.5)
    title('Ratio of cross-correlation to auto-correlation')
    xlabel('Sample'); ylabel('Magnitude'); grid on
    title('Ratio of cross-correlation to auto-correlation')
    xlabel('Sample'); ylabel('Magnitude'); grid on
    axis([1 L_R 0 1])
    pause
%% Removing AWGN (From Front of Received Signal)
rec_sig0 = yg_sv(1+L_AWGN:end); % Removing AWGN
rec_sig1 = rec_sig0/max(rec_sig0);
%% Time-Offset Estimation (Integer)
xx = zc;
yy = rec_sig0(1+l_zc_cp:L_ZC-L);
cor1 = xcorr(yy,xx,L, 'coeff');
% ===== %
figure(60)
    plot(0:length(cor1)-1,abs(cor1).^2, 'b', 'linewidth', 1.5)
    grid on
    title('Time-Offset Estimation')
    xlabel('Sample'); ylabel('Magnitude')
    axis('tight')
    pause
%% Generating Fractional time Offset %% (Arbitrary Inter)
L_IN = length(rec_sig1);
% ===== %
fs = L;
fpass = UPS*0.5;
fstop = UPS*3.5;
Np = 32;
h3 = remez(Np-2,[0 fpass fstop (fs/2)]/(fs/2),[1 1 0 0],[1 200]);
h3 = h3/max(h3);
hh3 = 32*h3;
% ===== %
P = 32;
Q = 3.0000000001;
P_Q = P/Q; % 32/5 input/output sample
rate P/Q
accum_a = 1;
in = 1;
out = 1;
wts_a = reshape([hh3 0],32,Np/32); % Polyphase Filter Weights
reg_a = zeros(1,Np/32); % Flush Filter Register
% % ===== %
dh = conv([hh3 0],[1 0 -1]/2); % Derivative Filter
dh = dh(2:length(dh)-1); % Adjusting Sample Indices
For (DPF)
dh1 = reshape(dh,32,Np/32); % Derivative Polyphase
Filter
% ===== %

```



```

while in <= L_IN
    reg_a = [rec_sig1(in) reg_a(1:(Np/32)-1)];
    while accum_a < 33 % Overflow counter
        int_a = floor(accum_a); % Nearest Neighbor
Replacement (Immediate Left)
        delta_a = accum_a-int_a; % Pointer Indices
        y3(out) = reg_a*wt_s_a(int_a,:)'+1*reg_a*delta_a*dh1(int_a,:); %
Inner Product (Filter with Input)
        out = out+1; % Output Index
        accum_a = accum_a+P_Q; % Accumulator
    end
    accum_a = accum_a-32; % Module(M=32)
    in = in+1; % Index Increments
end
% ===== %
y_a = y3(1:floor(Q):end);
y_b = y_a/max(y_a);
L_AR1 = length(y_a);
%% Arbitrary interpolator with 32 path polyphase filter%% (Fractional
Time-Offset)
L_AR2 = length(y_a);
P1 = 32;
Q1 = 4;
P_Q_1 = P1/Q1; % 32/4 input/output sample
rate P/Q
accum_b = 1;
in_b = 1;
out_b = 1;
wt_s_b = reshape([hh3 0],32,Np/32); % Polyphase Filter Weights
reg_b = zeros(1,Np/32); % Flush Filter Register
% ===== %
while in_b <= L_AR2
    reg_b = [y_a(in_b) reg_b(1:(Np/32)-1)];
    while accum_b < 32 % Overflow counter
        int_a = floor(accum_b)+1; % Nearest Neighbor
Replacement (Immediate Left)
        delta_b = accum_b-int_a; % Pointer Indices
        y4(out_b) = reg_b*wt_s_b(int_a,:)'+1*reg_b*delta_b*dh1(int_a,:); %
Inner Product (Filter with Input)
        out_b = out_b+1; % Output Index
        accum_b = accum_b+P_Q_1; % Accumulator
    end
    accum_b = rem(accum_b,32); % Module(M=32)
    in_b = in_b+1; % Index Increments
end
% ===== %
a = 2*Q1;
y_a1 = y4(a:Q1:end);
y_b1 = y_a1/max(y_a1);
L_ARR = length(y_a1);
% ===== %
L_ZC = length(zc_packet);
% ===== %
figure(72)
df = 4;
subplot(211)

```

```

plot(abs(rec_sig1(1+L:L+L/df)),...
'--sb','linewidth',1.5)
hold on
plot(abs(y_b(1+L:L+L/df)),...
'--r','linewidth',1.5)
hold off
title('Time Reponse of Signal W/O Time-Offset(Blue) V.S Signal W/
Time-Offset(red)')
axis('tight')
xlabel('Sample Index');ylabel('Magnitude')
grid on
% ===== %
subplot(212)
plot(abs(rec_sig1(1+L:L+L/df)),...
'--sb','linewidth',1.5)
hold on
plot(abs(y_b1(1+L:L+L/df)),...
'--r','linewidth',1.5)
hold off
title('Time Reponse of Signal After Time Offset Correction')
axis('tight')
xlabel('Sample Index');ylabel('Magnitude')
grid on
pause
%% Channel Estimation ** Zadoff-Chu Sequence**
L_ZC_CP = length(zc_cp);
zc_rx = y_a1(1+L_ZC_CP:L_ZC_CP+L+L); % Removing CP
ZC_EXT = [];
% ===== %
for n = 1:2
rec_zc = zc_rx((n-1)*L+1:n*L); % Extracting ZC-Seq
ZC_RX = fftshift(fft(rec_zc)); % Frequency Domain
EST_CH = ZC_RX./ZC_SYM; % Channel Estimation
% EST_CH(L/2) = 0;
rx_ch_comp = ZC_RX./EST_CH; % Removing Channel
Distortion
rx_ch_comp(L/2) = 0;
ZC_EXT = [ZC_EXT rx_ch_comp];
end
% ===== %
ZC_DC = ZC;
ZC_DC(32) = 0;
% ===== %
figure(75)
subplot(221)
plot(-N/2+1:N/2-1,1/590*abs(EST_CH(T)),'--r','linewidth',2)
hold on
plot(-N/2+1:N/2-1,abs(ZC_DC),'b','linewidth',1.5)
hold off
title('Estimated Channel(red)')
xlabel('Sample Index');ylabel('Magnitude');grid on
axis([-32 32 0 2])
% ===== %
subplot(222)
plot(rx_ch_comp,'r','linewidth',2)
hold on

```

```

plot(exp(1i*2*pi*1/(N-1)*(1:N-1)), 'linewidth',1)
hold off
title('Phase Response');
xlabel('In-Phase');ylabel('Quadrature')
axis('square');grid on
% ===== %
subplot(212)
plot(-(L/2-1):L/2,abs(rx_ch_comp), '-*k', 'linewidth',1.5)
title('Equalized Signal')
xlabel('Sample Index');ylabel('Magnitude');grid on
axis('tight')
pause

```